DENSITY MODEL CORRECTIONS DERIVED FROM ORBIT DATA TO CHARACTERIZE UPPER ATMOSPHERIC DENSITY VARIATIONS

BY

Travis Francis Lechtenberg

Submitted to the graduate degree program in Aerospace Engineering and the Graduate Faculty of the University of Kansas in partial fulfillment of the requirements for a doctoral degree.

Committee members

Chairperson:

Dr. Craig McLaughlin

Dr. Ray Taghavi

Dr. Saeed Farokhi

Dr. Dongkyu Choi

Dr. Thomas Cravens

Date

Presented:

The Dissertation Committee for Travis Lechtenberg certifies that this is the approved Version of the following Dissertation:

DENSITY MODEL CORRECTIONS DERIVED FROM ORBIT DATA TO CHARACTERIZE UPPER ATMOSPHERIC DENSITY VARIATIONS

Committee:

Committee members

Chairperson:

Dr. Craig McLaughlin

Dr. Ray Taghavi

Dr. Saeed Farokhi

Dr. Dongkyu Choi

Dr. Thomas Cravens

Date

Approved:

ABSTRACT

One goal of this research is to estimate density model corrections using readily available Satellite Laser Ranging (SLR) data, and to demonstrate this approach's validity for additional satellites with similar data sets in the future. The research also aims to utilize previously unused or little used sources of orbit state data to generate corrections to existing density models. These corrections yield estimated density corrections which lead to better drag estimates, improved orbit determination and prediction, as well as an enhanced understanding of density variations in the thermosphere and exosphere. This research primarily focuses on using SLR data. This examination will give a better idea of obtainable improvements in atmospheric density. Consideration will also be given to the effects of varying levels of geomagnetic and solar activity.

This work established the validity of using SLR data to estimate atmospheric densities by comparing results for the ANDE Castor satellite to results for the CHAMP and GRACE satellites for the same time periods. The density correction factors and standard deviations comparing the baseline model densities to the derived atmospheric densities are also examined for the ANDE Castor satellite. For the entire family of ANDE satellites, the uncertainty in atmospheric density is established for each arc. The uncertainties are significantly higher at the beginning of the arc for each of the satellites, and the uncertainties also increase as the satellites drop in altitude. Preliminary density values for the Special Purpose Inexpensive Satellite (SPINSat) are also derived.

TABLE OF CONTENTS

NOMENCLATURE

Symbol	Definition	Units
$\vec{a}$	acceleration vector due to atmospheric drag	m/s^2
a_p	geomagnetic 3-hourly planetary equivalent amplitude index	gamma, Tesla, or kg s m^{-1}
A	satellite cross-sectional area	m^2
A_p	geomagnetic daily planetary amplitude index	gamma, Tesla, or kg s m^{-1}
$\Delta B/B$	estimated ballistic coefficient correction	~
BC	ballistic coefficient	m^2/kg
c_D	satellite drag coefficient	~
d	cross correlation delay	
$F_{10.7}$	daily solar radio flux measured at 10.7 cm wavelength	SFU
$\overline{F}_{10.7}$	$F_{10.7}$ running 81-day centered smoothed data set	SFU
$\overline{F}_S$	Jacchia-Bowman 2008 new solar index	SFU

g_o	gravitational acceleration	m/s^2
Δh	altitude change	m
i	cross correlation series index	
j	user defined Gauss-Markov correlated half-life time series index	
k	Gauss-Markov sequence index	
K_p	geomagnetic planetary index	~
$M_{10.7}$	solar proxy for far ultra-violet radiation	SFU
$\bar{M}_{10.7}$	$M_{10.7}$ running 81-day centered smoothed data set	SFU
m	satellite mass	kg
mx	mean of series x	
my	mean of series y	
M	mean molecular mass	amu
N	number of elements	
Δp	atmospheric pressure change	N/m^2
p_o	absolute pressure	N/m^2
$\hat{P}$	filter covariance matrix	
$\tilde{P}$	smoother covariance matrix	
$\bar{P}$	differenced covariance matrix	

r	cross correlation coefficient	
$\vec{r}$	satellite position vector	m
R	universal gas constant	J K^{-1} mol^{-1}
$\vec{R}$	McReynold's consistency test ratio	
$S_{10.7}$	solar extreme ultra-violet radiation at 26-34 nm wavelength	SFU
$\overline{S}_{10.7}$	$S_{10.7}$ running 81-day centered smoothed data set	SFU
t	time	S
T	temperature	K
v_{rel}	satellite velocity magnitude relative to Earth's atmosphere	m/s
$\vec{v}_{rel}$	satellite velocity vector relative to Earth's atmosphere	m/s
$w(t)$	Gaussian white random variable	
x	x component of satellite position vector	m
x	Gauss-Markov process dynamic scalar random variable	
x	cross correlation series	
ΔX	state error	

$\Delta\hat{X}$	optimal state error estimate	
$\boldsymbol{X}$	satellite state vector	
$\bar{X}$	difference state vector	
$\bar{X}_{filter}$	filter state estimate	
$\bar{X}_{smoother}$	smoother state estimate	
Δy	measurement residual	
y	y component of satellite position vector	m
y	cross correlation series	
Y_{10}	mixed solar index	SFU
z	z component of satellite position vector	m

Greek Letters	Definition	Units
α	Gauss-Markov process variable	
$\Delta\rho/\rho$	estimated atmospheric density correction	~
ρ	atmospheric density	kg/m^3
$\vec{\sigma}$	denominator for McReynold's consistency test ratio	
σ_w^2	variance of Gaussian white random variable	
τ	user defined correlated half-life	
ω_{Earth}	Earth's angular velocity magnitude	rad/s
$\vec{\omega}_{Earth}$	Earth's angular velocity vector	rad/s
Φ	transition function	

Abbreviations	Definition
CC	Cross Correlation
CHAMP	Challenging Minisatellite Payload
CIRA	COSPAR International Reference Atmosphere
COSPAR	Committee on Space Research
CNES	Centre National d'Études Spatiales
DCA	Dynamic Calibration of the Atmosphere
DORIS	Doppler Orbitography by Radiopositioning Integrated on Satellite
Dst	Disturbance Storm Time index
DTM	Drag Temperature Model
ESA	European Space Agency
EUV	Extreme Ultra-Violet
GEOSAT	Geodetic Satellite
GFO	GEOSAT Follow-On
GOES	Geostationary Operational Environmental Satellites
GPS	Global Positioning System
GRACE	Gravity Recovery And Climate Experiment
GSFC	Goddard Space Flight Center

HASDM	High Accuracy Satellite Drag Model
ICESat	Ice, Cloud, and Land Elevation Satellite
MSISE	Mass Spectrometer Incoherent Scatter Extending from ground to space
MUV	Middle Ultra-Violet
NASA	National Aeronautics and Space Administration
NOAA	National Oceanic and Atmospheric Administration
NRLMSISE	Naval Research Laboratory Mass Spectrometer Incoherent Scatter Extending from ground to space
ODTK	Orbit Determination Tool Kit
POE	Precision Orbit Ephemerides
PSO	Precision Science Orbit
RMS	Root-Mean-Squared Value
RSO	Rapid Science Orbit
SBUV	Solar Backscatter Ultraviolet
SEE	Solar Extreme-ultraviolet Experiment
SEM	Solar Extreme-ultraviolet Monitor
SETA	Satellite Electrostatic Triaxial Accelerometer
SFU	Solar Flux Units
SLR	Satellite Laser Ranging

SOHO	Solar and Heliospheric Observatory
SOLSTICE	Solar/Stellar Irradiance Comparison Experiment
SORCE	Solar Radiation and Climate Experiment
STAR	Spatial Triaxial Accelerometer for Research
TAD	Traveling Atmospheric Disturbance
TIMED	Thermosphere Ionosphere Mesosphere Energetics and Dynamics
TLE	Two Line Element
UARS	Upper Atmosphere Research Satellite
XRS	X-Ray Spectrometer

LIST OF FIGURES

LIST OF TABLES

1 Introduction

1.1 Objective

One goal of this research is to estimate density model corrections using readily available Satellite Laser Ranging (SLR) data, and to demonstrate this approach's validity for additional satellites with similar data sets in the future. The research also aims to utilize previously unused or little used sources of orbit state data to generate corrections to existing density models. These corrections yield estimated density corrections which lead to better drag estimates, improved orbit determination and prediction, as well as an enhanced understanding of density variations in the thermosphere and exosphere. This research primarily focuses on data available via SLR data. This examination will give a better idea of obtainable improvements in atmospheric density. Consideration will also be given to the effects of varying levels of geomagnetic and solar activity.

1.2 Motivation

The extreme upper atmosphere, including the thermosphere and exosphere is extremely variable, more so than predicted by current density models. The variations in density magnitude and atmosphere composition at these altitudes can adversely affect the determination and prediction of satellite orbits. Improved orbit determination techniques can be used to help prevent satellite collisions, predict satellite life-spans, and predict satellite reentry times. Several satellite activities require precise knowledge of the satellite's location and velocity; orbit determination techniques aid in the accurate and precise determination of the satellite's state.

Atmospheric density is one of the largest uncertainties in orbit determination and prediction at low altitudes; it is also one of the primary variables in the calculation of drag on orbiting bodies. Drag is also affected by variables such as the cross sectional area of the orbiting

body (A), the mass of the orbiting body (m), and the velocity of the satellite (v). Other perturbing variables, such as Earth's gravitational field and solar-radiation pressure, are smaller sources of uncertainty than the neutral atmospheric density.

The Earth's atmospheric density is influenced by several effects. The largest influences on atmospheric density are from direct heating from the sun through extreme-ultraviolet (EUV) radiation and the interactions between the atmosphere, the Earth's magnetic field, and charged particles emitted by the sun.

Data used in the model calculations for atmospheric density for magnetic field and solar flux are measured and distributed as averaged three-hour or daily global values. These time scales are generally too large to account for rapid short-term variations in the atmosphere, but are more useful for determination of atmospheric density of larger timescales such as ones examined in this study.

Current density models require corrections to construct a more accurate understanding of thermospheric and exospheric densities and atmospheric density variation to determine and predict orbits of individual orbiting bodies. These corrections can be estimated using precision orbit ephemerides (POEs) as well as SLR data available for specific satellites.

Using these estimates of atmospheric density, better models of the drag forces that act upon satellites may be produced in the future. As the accuracy of the density models improve, so too will the drag models. Orbit determination can be significantly improved through these corrections, as drag is one of the primary perturbing forces for low Earth orbiting (LEO) satellites, particularly for orbits for very low altitude satellites. Improved orbit determination leads to better knowledge of a satellite's operational life, its time and location of reentry, as well as future satellite position prediction. This research also brings about a better understanding of how the space environment and weather affect atmospheric density. Currently, knowledge of

solar and geomagnetic effects on the atmosphere and exosphere is incomplete; better measurement of density and its variations will facilitate continued study of these effects.

Eventually, this research intends to increase the accuracy of satellite drag calculations, as well as improve understanding of the thermosphere wherein most satellites orbit. The immediate goal of this research is to demonstrate the effectiveness of using the Atmospheric Neutral Density Experiment (ANDE) orbital satellite laser ranging (SLR) measurements and post-processed data to formulate corrections to existing atmospheric density models. These corrections can be used to generate better atmospheric drag calculations, which will improve the accuracy of orbit determination and prediction, as well as increasing understanding of density variations in the upper thermosphere and exosphere.

1.3 Satellite Drag

Information on satellite drag characteristics can be found in Vallado [2007][1]. There are two primary perturbations that affect LEO satellites, the first is acceleration due to atmospheric drag, and the second is additional accelerations due to the oblateness of the earth (J2), and other higher order gravity terms. As the altitude of a satellite decreases, drag becomes a larger and larger factor in the perturbation of a satellite's orbit. After these two forces, the next most significant sources of perturbation are from solar radiation pressure, Earth albedo, and third body effects from bodies such as the Moon and Sun. Drag is occasionally used for orbit maintenance through aerobraking and tethers which aid in satellite orientation, though in general, drag is regarded primarily as a hindrance to the satellite's life span. Satellites at higher altitudes are proportionately more affected by third body effects and solar radiation pressure, as the effects of atmospheric density decrease exponentially with increases in altitude. The continually increasing role of LEO satellites, in both the public and private sectors has led to large amount of research being directed towards the comprehension of the upper atmosphere and its interactions with these satellites in the form of drag. This research will presumably lead to more accurate atmospheric

density models, which will aid in future satellite mission planning. There are three primary goals for modeling drag: first is determining the orbit of the satellite, the second is estimating satellite lifetime, and the third is to determine physical properties of the atmosphere.

Drag is the process through which an object's velocity is altered by the collision of atmospheric particles against its outer hull, which due to the conservation of momentum detract from the velocity of the satellite and transfer momentum to atmospheric particles. This force is non-conservative as the total mechanical energy of the satellite changes due to this interaction with the atmosphere. The majority of the momentum change is localized around periapsis, which reduces the satellites semi-major axis and eccentricity, slowly altering the satellites orbital path to approach a circular orbit.

According to Vallado [2007]1 a complete model of atmospheric perturbations must include knowledge of molecular chemistry, thermodynamics, aerodynamics, hypersonics, meteorology, electromagnetics, planetary sciences, and orbital mechanics. Analysis of satellite drag requires a thorough understanding of atmospheric properties. One way of measuring drag is to measure accelerations induced upon the satellite and attempt to isolate the acceleration due to drag, which occurs along the satellite's track. The following equation describes the relationship between acceleration drag forces, and the independent variables of atmospheric density and velocity. Other variables are generally grouped together for the purpose of determining the acceleration due to drag into a quantity known as ballistic coefficient.

$$\vec{a} = -\frac{1}{2}\frac{c_D A}{m}\rho v_{rel}^2 \frac{\vec{v}_{rel}}{|\vec{v}_{rel}|} \tag{0.1}$$

The drag coefficient c_D is a dimensionless quantity describing the effect that drag has on the satellite and is based largely on the satellite's configuration. The dependence on satellite

configuration and variability of the atmosphere's characteristics mean that the drag coefficient for the satellite is typically estimated. Drag coefficients for satellites in the upper atmosphere are typically approximated as 2.2 for flat plates, and 2.0 to 2.1 for spherical bodies. At most, the drag coefficient is estimated to 3 significant figures. The difficulties that arise from complex satellite configurations require further improvements in satellite drag determination to be researched.

The symbol, ρ, denotes atmospheric density, the concentration of atmospheric particles in a given volume. Density can be one of the more difficult parameters to approximate for a satellite drag situation due to variability of the satellite's cross-sectional area, A, and uncertainties in c_D. The variability of A is primarily due to constantly changing attitudes of satellites lacking attitude control. A better approximation of A and therefore ρ may be obtained if the attitude and geometry of the satellite at various points in time are more accurately known. Mass, m, can also be variable over a given amount of time due to orbit maintenance maneuvers, as well as accumulated atmospheric particles that can bond to the surface of the satellite. The relative velocity vector $\vec{v}_{rel}$ is defined as the velocity vector relative to the rotating Earth's atmosphere and can be determined by the following equation1.

$$\vec{v}_{rel} = \frac{d\vec{r}}{dt} - \vec{\omega}_{Earth} \times \vec{r} = \left[\frac{dx}{dt} + \vec{\omega}_{Earth} y \frac{dy}{dt} - \vec{\omega}_{Earth} x \frac{dz}{dt} \right]^T \tag{0.2}$$

The atmosphere of the Earth rotates with the Earth, with a velocity profile in which the atmosphere moves most quickly close to the surface of the earth and decreases in speed with altitude. Satellites are subject to both this general motion, as well as atmospheric winds. This atmospheric motion generates side and lifting forces, as well as drag forces. The drag forces are defined as being along the velocity vector of the satellite relative to the atmosphere.

Another way of representing the satellites susceptibility to drag is through the ballistic coefficient (BC). There have been multiple definitions of ballistic coefficient over the years, so clarity of definition is important. The traditional definition of ballistic coefficient, a remnant from the days of muskets and cannons is defined as follows.

Classical Definition

$$BC = \frac{m}{c_D A} \tag{0.3}$$

The definition used by the Orbit Determination Tool Kit (ODTK), the software primarily used for this research, the definition used by Bruce Bowman[2], and the definition that will be referred to for the rest of this document, however, is this inverse of this relationship.

Definition in this document

$$BC = \frac{c_D A}{m} \tag{0.4}$$

Using this definition, a lower value of BC equates to drag having less of an effect on the given satellite instead of more as in the classical definition.

Static and time varying atmospheric models rely on two relationships that are core to understanding how pressure and density change within the atmosphere1. The first is the ideal gas law.

$$\rho = \frac{p_o M}{g_o R T} \tag{0.5}$$

The ideal gas law characterizes the basic interactions between atmospheric pressure p_o, the mass of the atmospheric constituents M, gravitational acceleration g_o, the universal gas constant R, and the temperature of the atmosphere T. As the Earth rotates throughout the day, different portions of the atmosphere are exposed to the sun's rays, which heat the atmosphere. This heat drastically affects atmospheric density through interactions with both the pressure and density of the gases in the upper atmosphere. Atmospheric densities observed on the lit side of the Earth are significantly greater than those found on the unlit side and this connection between temperature and density is of great importance as it is the single largest cause of variation in atmospheric density on a daily basis.

The second equation is the hydrostatic pressure equation which characterizes the change in pressure found to result from changes in height. The hydrostatic equation is defined below.

$$\delta p = -\rho g \delta h \tag{0.6}$$

These two relationships are paramount to understanding the complex interactions in atmospheric density. Both equations demonstrate the interdependency of pressure and density values. Through these two relationships, much of the atmosphere may be characterized.

1.4 Atmospheric Density Models

The following section is primarily a summary of information found in Vallado [2007]1, which contains an introduction to commonly used atmospheric density models. Additional information on the neutral atmosphere may also be found in Vallado [2007]1. Most atmospheric models are developed using one of two approaches. 1) Using laws of conservation as well as models of the atmospheric constituents to create a physical model of the atmosphere. 2) Using simplified physical concepts in conjunction with in-situ measurements and satellite tracking data. The models are also divided into static and time-varying models.

Time varying models are generally the most accurate and complete, but require accurate data for different times and conditions, and are generally computationally expensive. A simple static exponential model can turn out to be relatively accurate for a given time while being much less expensive computationally.

Models examined in this research include: Jacchia 1971[3], Jacchia-Roberts[4], Committee on Space Research (COSPAR) International Reference Atmosphere (CIRA 1972)[5], Mass Spectrometer Incoherent Scatter (MSISE 1990)[6], and Naval Research Laboratory Mass Spectrometer Incoherent Scatter (NRLMSISE 2000)[7]. The "E" suffix on the last two models indicates that these are extended models in that they reach from sea level to space.

1.4.1 Solar and Geomagnetic Indices

Two major forcing conditions behind variability in atmospheric densities are solar and geomagnetic activity. Solar activity accounts for most of the variability in the upper atmosphere. These variations are caused by atmospheric heating that occurs due to the absorption of EUV radiation. Since almost all incoming radiation is absorbed by the atmosphere, little of this EUV radiation reaches the Earth's surface, and a proxy index is used to measure the amount of radiation incoming to the earth in the form of 10.7 cm wavelength electromagnetic radiation

($F_{10.7}$). The $F_{10.7}$ wavelength is typically represented in models as an 81 day running average denoted by $\overline{F}_{10.7}$. The 10.7 cm wavelength and EUV radiation have been found to both originate from the same layers of the sun's chromosphere and corona giving validity to using the 10.7 cm wavelength as a proxy. Some satellites are equipped to measure EUV flux directly, but the only model to currently incorporate these readings is the Jacchia-Bowman model[8]. $F_{10.7}$ has been regularly recorded since 1940 in Solar Flux Units (1 SFU = 10^{-22} W m^{-2} Hz^{-1}), and typical values range from 70-300 SFU for any given day. Measurements of solar flux are distributed daily by the National Oceanic and Atmospheric Administration (NOAA) at the National Geophysical Data Center in Boulder, Colorado. From 1947 until 1991, measurements were taken at 1700 UT at the Algonquin Radio Observatory in Ottawa, Ontario. Since then, measurements have been taken at the Dominion Radio Astrophysical Observatory in Penticton, British Columbia. Measurements of solar flux can be found at the National Geophysical Data Center's website[9].

Variations in the earth's magnetic field can affect satellites in numerous ways. First, the charged particles cause ionization in the upper atmosphere. Second, the charged particles alter the attractive forces experienced by the satellite. Third, ionization interferes with satellite tracking and communication. Finally, variations in the magnetic field can interfere with onboard magnets used for attitude adjustment.

Geomagnetic activity is measured to determine atmospheric heating by a quasi-logarithmic geomagnetic planetary index denoted as K_p. The K_p index is a worldwide average of geomagnetic activity below the auroral zones. Measurements of K_p are taken every 3 hours from 12 locations worldwide. The geomagnetic planetary amplitude, a_p, is a linear equivalent of the K_p index, and is a 3-hourly index, which is averaged to a daily planetary amplitude A_p. Planetary amplitude is measured in gamma, defined as:

$$gamma = 10^{-9} Tesla = 10^{-9} \frac{kg \cdot s}{m} \quad (0.7)$$

Values for planetary amplitude range from 0 to 400, though values rarely exceed 100 and average at about 10-20. Geomagnetic activity has two primary cycles, the first mirrors the 11 year solar cycle with maxima occurring during the declining phases of the solar cycles. The second is a semi-annual cycle due to the variability of the solar wind's incidence with the Earth's magnetosphere. Data on geomagnetic planetary indices and planetary amplitudes is available at the National Geophysical Data Center's Website[10].

Solar and geomagnetic activity can be separated into bins as defined in Picone et al. [2002]7 as:

Table 1: Defined Solar and Geomagnetic Activity Bins

$F_{10.7}$ Solar Activity		A_p Geomagnetic Activity	
Low	$F_{10.7}<75$	Quiet	$A_p<10$
Moderate	$75<F_{10.7}<150$	Moderate	$10<A_p<50$
Elevated	$150<F_{10.7}<190$	Active	$50<A_p$
High	$190<F_{10.7}$		

1.4.2 Jacchia 1971 Atmospheric Model

The Jacchia 1971 atmospheric model was created as a replacement for the model proposed the previous year, the Jacchia 1970 model. The model was updated in an attempt to meet the composition and density data derived from mass spectrometer and EUV-absorption data, with ranges from altitudes of 110-2000 km.3 The model begins analysis by assuming a boundary atmospheric condition at 90 km and that discrepancies in the mean molecular mass below 100 km

are due to dissociation of oxygen molecules. From 90-100 km, an empirical model of the mean molecular mass is used, and from 100-150 km a diffusive model is used until the ratio of O/O_2 reaches 9.2.3 Above 125 km, the atmosphere is modeled with a temperature profile where the temperature approaches an asymptotic value of the exospheric temperature. To even out shorter term variations, such as the 27 day solar, cycle, the model is adapted to use a running 81 day average for geomagnetic and solar activity levels.

1.4.3 Jacchia-Roberts Atmospheric Model

Largely based upon prior work done for the Jacchia 1970 model, the Jacchia-Roberts atmospheric model determines exospheric temperature using analytical expressions based on functions of position, time, solar activity, and geomagnetic activity4. Density is then empirically determined from atmospheric temperature profiles, or from the diffusion equation. Roberts modified the 1970 model by using partial fractions to integrate from 90-125 km, and used a different asymptotic function from Jacchia's 1971 model in order to achieve an integrable form 4.

1.4.4 CIRA 1972 Atmospheric Model

An atmospheric model is periodically released by the Committee on Space Research (COSPAR); releases began in 1965 and the model was updated in 1972 to incorporate the findings of the Jacchia 1971 model, as well as mean values for low altitudes (25-500 km), satellite drag, and ground based measurements5. The model is semi-theoretical, but leaves some free variables.

1.4.5 MSISE 1990 Atmospheric Model

The MSIS series of models are formulated utilizing mass spectrometer data from satellites, as well as incoherent scatter radar from ground based sites. In addition, data is used from the Drag Temperature Model (DTM), which is based on air-glow temperatures6. The advantages posed by the MSIS models over modified Jacchia-Roberts models are that the MSIS

models take into account a greater amount of data than was available during the creation of the Jacchia-Roberts model, and that these models tend to require smaller amounts of code. The modified Jacchia-Roberts model does outperform this model in certain situations though.

1.4.6 NRLMSISE 2000 Atmospheric Model

The newest release in the MSIS line is the NRLMSISE 2000 model, released by the Naval Research Laboratory, which incorporates satellite drag data using spherical harmonics over two complete solar cycles7. Both MSISE models require less code in order to determine the atmospheric densities, though Jacchia-based models tend to perform better in certain scenarios, and have the advantage of being less computationally expensive.

1.4.7 Jacchia-Bowman Atmospheric Models

The Jacchia-Bowman models are derived from Jacchia's diffusion equations, and are intended to reduce density errors by using solar indices, improved semiannual density variation models, and a geomagnetic index algorithm. The newest version of the Jacchia-Bowman model utilizes data from both ground based observations, as well as on-orbit satellite data to calculate thermospheric and exospheric temperatures, which are used to generate density values. Further details apart from those espoused here can be found in Bowman et al. [2008]8.

The newest model uses a combination of four measurements of solar flux to better model semiannual seasonal variations that can be observed peaking in April and October, and attaining minima in January and July. The October maximum, and July minimum are observed as being more pronounced than the April maximum, and January minimum. The Jacchia-Bowman model uses a previously defined function for the atmospheric density that is a relationship between density, time, amplitude and height as a baseline for attempting to better model this semiannual variation.

Typically, the ultraviolet solar flux is estimated using measurement of the 10.7 cm wavelength, which serves as a proxy for EUV activity. $F_{10.7}$ values tend to bottom out during solar minimum, thus creating a need for the Jacchia-Bowman model to incorporate other models of solar activity.

To account for solar activity after $F_{10.7}$ values bottom out, three other sources of measuring solar activity were used in the Jacchia-Bowman model. In December 1995, NASA/ESA launched the Solar and Heliospheric Observatory (SOHO) which uses an instrument dubbed the Solar Extreme-ultraviolet Monitor (SEM). This device measures wavelengths of 26-34 nm, and converts the measurements to SFU. This index is useful for measuring EUV line emissions and is denoted by S_{10} or $\overline{S}_{10}$ for 81-day running averages.

NOAA's series of operational weather satellites are equipped with a Solar Backscatter Ultraviolet (SBUV) spectrometer that is most commonly used to monitor ozone in the lower atmosphere. In its discrete operating mode, the SBUV measures MUV radiation near the 280 nm wavelength, which is near the Mg *h* and *k* lines. This allows the index to measure the chromospheric and a portion of the photospheric solar active region activity. Linear regression of the $F_{10.7}$ index is used to attain the M_{10} index used here.

The GOES X-ray spectrometer (XRS) instrument provides data for the last of the solar indices used in the Jacchia-Bowman model. The XRS measures X-rays in the 0.1-0.8 nm range. X-rays at these wavelengths are a major energy source during periods of high solar activity, but during periods of low to moderate solar activity hydrogen (H) Lyman-α dominates. Lyman-α values are obtained from the SOLSTICE instrument on the UARS and SORCE NASA satellites as well as by the SEE instrument on NASA TIMED research satellite. The SFU values of both the X_{10} and Lyman-α measurements are weighted towards X_{10} values during periods of high solar activity, and towards the Lyman-α values during periods of moderate to low solar activity to create a mixed solar index known as Y_{10}.

To estimate thermospheric temperatures, the Jacchia-Bowman model used a weighted indexing scheme that incorporated both $\overline{F}_{10}$ and $\overline{S}_{10}$ data, and is denoted as $\overline{F}_S$.

$$\overline{F}_S = \overline{F}_{10} W_T + \overline{S}_{10}\left(1 - W_T\right) \tag{0.8}$$

where:

$$W_T = \left(\overline{F}_{10} / 240\right)^{1/4} \tag{0.9}$$

The Jacchia-Bowman model uses this index as well as the delta values between the daily values and running 81-day averages for all four previously referenced indexes to determine thermospheric densities. The newest model does a better job of measuring decreases in density during the solar minimum, though it does not completely capture the density variation. The Y_{10} index was recently added in the latest (2008) model and accounts for differences observed between the 2008 and 2006 variations of the model.

In addition to modeling indices of solar activity, the Jacchia-Bowman model also attempts to model changes in the atmosphere caused by geomagnetic storms. The Disturbance Storm Time (Dst) index is used as an indicator of the strength of the storm-time ring current in the inner magnetosphere. Most magnetic storms begin with a sharp rise in Dst due to increased pressure from the solar wind. Following this, the Dst decreases drastically for the duration of the storm as ring of current energy increases during the storm's main phase, funneling energy along magnetic field lines. During recovery phase, Dst increases back to normal levels as ring current energy decreases. Dst is considered a more accurate measure of energy deposited in the thermosphere by Bowman than the standard a_p index measured by high latitude observatories.

The model formulated by Bruce Bowman considers Dst more accurate because observatories may be blinded to energy input during storms and thus underestimate the effect of geomagnetic storms on the atmosphere.

1.4.8 Russian GOST Model

The GOST model is an analytical model developed during the Soviet era to determine atmospheric densities from observations of Cosmos Satellites[1]. The model has been used for nearly 30 years, and is still incorporating satellite measurements to this day1. The GOST model is able to disregard specified parameters easily by omitting them from the calculation; this property allows the GOST to gain its estimates very quickly, and reduce required computer resources1.

1.5 Previous Research on Atmospheric Density Model Corrections

There are two methods of research currently in use to address the problems of modeling atmospheric density for the purpose of determining satellite drag. The first is though Dynamic Calibration of the Atmosphere (DCA), and the second is through the analysis of accelerometer data from satellites themselves.

1.5.1 Dynamic Calibration of the Atmosphere

Dynamic Calibration of the Atmosphere (DCA) is a technique for improving or correcting existing atmospheric models and their corresponding densities. DCA provides information about density variations in the atmosphere and the statistics of these variations1. DCA techniques have been used since the early 1980's and are an area of ongoing research in applications of orbit determination. DCA modeling techniques estimate density corrections every three hours to maintain consistency with initial work performed by Nazarenko in the 1980's. DCA methods originally determined density from empirical inputs as opposed to observed geomagnetic data which was judged unreliable in the early 1980's. Approaches with access to

excellent data make corrections on a 3-hourly basis, while those that rely primarily on TLE sets are only capable of generating daily corrections. DCA techniques use an input of a "true" ballistic coefficient in order to determine density corrections to models; these corrections are usually made to variants of Jacchia-71 and MSIS models1. There have been several usages of the DCA approach in recent years.

Storz et al. [2005][11] incorporated data from 75 inactive payloads and debris to solve for corrections to thermospheric and exospheric neutral density for altitudes between 200-800 km. Corrections were regularly made every three hours and densities could be predicted up to three days in advance using predictions of $F_{10.7}$ solar flux. Storz et al. [2005][11] improved upon DCA techniques by using prediction filters, and using a segmented solution for ballistic coefficient techniques to achieve density accuracies that were within a few percent of true densities.

Bowman et al. [2004][2] describe a method for determining daily atmospheric density values by basing them upon satellite drag data. A differential orbit correction program using special perturbations orbit integration was applied to radar and optical observations of satellites to obtain 6-state element vectors, as well as the ballistic coefficients for the satellites observed in this study. The states were integrated from the modified Jacchia 1970 model that was also utilized for the High Accuracy Satellite Drag Model (HASDM). Daily temperature and density values were calculated using computed energy dissipation rates. These temperatures were verified by examining daily values of satellites as obtained by this DCA examination in comparison to values obtained from the HASDM DCA program. The densities were verified by comparing them against historical data for the past thirty years.

The goal of Bowman [2004][12] was to represent the observed semiannual density variation of the last 40 years. The study took historical radar observational data of 13 satellites with perigees ranging from 200-100 km. Using this historical data, accurate daily density values at perigee have been found by relating the density to energy dissipation rates. The study was able to

observe the semiannual variation, as well as characterize variations due to altitude and solar activity.

Cefola et al. [2003][13] estimated corrections to the GOST atmospheric model using data from Two Line Element (TLE) sets. These density corrections were made using a bias term, as well as a linear altitude grid. The model uses input in the form of TLE data from 300-500 satellites in LEO orbit, in addition to observed solar flux and geomagnetic data. The model was examined over a period of 10 months in the later part of 2002 and early 2003. The paper demonstrates the capability to monitor density variations given satellite TLEs in nearly real time.

Yurasov et al. [2004][14] also used TLEs to assess density corrections. These TLEs were taken from inactive objects in LEO orbit. Again, density was given a linear relationship with altitude. Hundreds of satellites were observed and then used to determine density. The accuracy of these densities was judged by comparison of orbit determination and predictions obtained with and without the estimated density corrections.

Yurasov et al. [2008][15] used DCA techniques as well as density corrections to better estimate reentry times for spacecraft. In this instance, corrections were made to the NRLMSISE 2000 model. This study considered both spherical and non-spherical objects in orbit around the earth. Reentry predictions increased in accuracy in this study, though the effect was more pronounced for spherical satellites which had unvarying BCs.

Wilkins et al. [2006][16] estimated corrections to the NRLMSISE 2000 model in an effort to improve orbit determination and prediction. The study acknowledged the limitations of using purely statistical corrections to atmospheric density, while still demonstrating marked improvement over baseline density models.

Wilkins et al. [2007a][17] sought to improve upon existing DCA techniques based on observations during the validation of Russian DCAs. The study found that successive

refinements using a series vanishing coefficients could remove errors from the solution. Each refinement used the previous refinement as a starting point as its basis and the process continued until improvements were no longer made. The primary goal of this study was to reduce residual errors in the calculation of drag.

Wilkins et al. [2007b][18] compares results from using DCA techniques in conjunction with the NRLMSISE model to results obtained from Nazarenko and Yurasov in their DCA based atmospheric density correction. The study examined two 4-year periods with varying levels of geomagnetic and solar activity; the first was from 11/30/1999-11/30/2003, and the second from 1/1/1995-6/1/2000. The study used data from 477 satellites in LEO orbit to derive corrections, and found that the models were valid, and proved that DCA is an effective method for determining corrections to current atmospheric density models.

DCA, though an extraordinarily useful tool, has limitations. DCA approaches are limited to localized time periods for which the DCA technique is applied. In order to correctly anticipate satellite orbit behavior, constant updates on atmospheric density are required, as well as archival knowledge of previous density corrections. DCA approaches also suffer from limited spatial and temporal resolution. The corrections take place on time scales of hours or days, and are ill suited for measuring short term variations in the thermosphere. This lack of temporal resolution is introduced by the usage of daily flux values, and 3-hour geomagnetic indices. Atmospheric variations cannot be represented during the averaged intervals of these indices. Another area of weakness for the DCA approach is the reliance on TLEs; though TLE data for LEO objects is plentiful, it lacks accuracy in regards to atmospheric density. HASDM2[,11,12] uses radar observations of LEO objects to obtain better density accuracies, though radar accuracy pales in comparison to that achievable by Precision Orbit Ephemerides (POE) or Satellite Laser Ranging (SLR), and is not generally available to parties outside the Department of Defense.

Research by Mance et al. [2009][19] examined application of DCA techniques to GEODYN, the NASA GSFC Precision Orbit Determination and Geodetic Parameter Estimation Program. Density corrections were applied to the NRLMSISE 2000 model with the intent of improving orbit precision of the GEOSAT Follow-On (GFO). The results were compared to the MSIS-86 model for a range of solar and geomagnetic activity levels. Results showed little improvement over the existing MSIS-86 model at 800 km, though corrections valid up to 800 km could yield improved results[19].

Doornbos et al. [2008][20] endeavored to use TLE data to calibrate thermospheric neutral density models. This study uses the large amount of available TLE data to calibrate density models with a lag of but a few days. The study tested two separate calibration schemes on a batch of 50 satellites during the year 2000. One calibration technique applied height-dependent scale factors to the density, and the other made corrections to the CIRA 1972 model temperatures, both of which effect significant changes to the physical density model. The errors were reduced in this study from 30% for raw empirical models to 15% for corrected models.

1.5.2 Accelerometers

Another way of measuring atmospheric drag is through the use of accelerometers onboard spacecraft in LEO. Recently, accelerometer accuracy has increased to the point where density can be estimated using the drag equation and measuring non-conservative forces. These accelerometers temporarily decrease in usefulness when orbit station keeping and attitude correction maneuvers are being made as these activities introduce additional forces into the accelerometer's analysis. In LEO, drag dominates as the primary non-conservative force; however, several other non-conservative forces exist such as solar radiation pressure, Earth albedo, and Earth infrared radiation. Accurate measurements of solar flux and earth radiation pressure can allow the non-drag terms to be accurately calculated using data received from accelerometers. So far, very few satellites have been equipped with accelerometers that are

sufficiently sensitive to measure atmospheric drag, and hence atmospheric density. Two of the few satellites currently equipped with accelerometers of sufficient accuracy are the CHAMP and GRACE satellites. Accelerometers have almost exact opposite general characteristics from two-line element sets in that they are highly accurate, though data sets are limited. Two-line element sets tend to be readily available for many satellites, yet are relatively inaccurate.

Konig and Neumayer [2003][21] and Bruinsma and Biancale [2003a][22] detail techniques used to derive atmospheric densities from accelerometer readings. Bruinsma and Biancale [2003b][23] and Bruinsma et al. [2004][24] give accelerometer data derived using these techniques.

Konig and Neumayer [2003][21] demonstrated the capability of the CHAMP accelerometer to measure major thermospheric events such as coronal mass ejections (CME) impinging the Earth's atmosphere. The study used accelerometer data to model non-conservative forces instead of relying upon models as the accelerometer is much more precise. Though precise, the accuracy of these measurements from accelerometers is suspect and it was judged the accelerometers likely require calibration and independent verification of data through either POEs or SLR data if this accelerometer data was to be used in subsequent studies.

Bruinsma and Biancale [2003a][22] found that total atmospheric density could be determined using the accelerometer data with the help of accurate force models for other non-conservative forces such as radiative effects. The study acknowledged the susceptibility of density readings to atmospheric wind in along-track directions which can increase or decrease the perceived density. The densities could also be affected by systematic bias due to uncertainty in the drag coefficient model as CHAMP's configuration is rather complex for drag coefficient determination. Initial results showed a very high accuracy in determining atmospheric density, which was projected to improve still further with the addition of more data points, as well as better density estimation techniques.

Bruinsma and Biancale [2003b][23] described the process through which atmospheric density may be determined given accelerometer readings. The CHAMP satellite provides decent geographical and altitude coverage during the course of its allotted 5-year lifespan due to its high-inclination orbit. The data required correcting for orbital maneuvers, specific events, and instrumental bias. The total density was then calculated using a 15-plate model for the drag coefficient. Accuracy was dependent on uncertainties in accelerometer calibration parameters and the aerodynamic coefficient, as well as the geomagnetic activity at the time in question.

Bruinsma et al. [2004][24] details the accuracy and limitations of the accelerometer aboard the CHAMP spacecraft and addresses issues with instrumental bias, scale factors, various modeling approaches, and density retrieval issues. The study analyzed data over the course of 21 months, and accumulated 1.2 million observations spanning all manner of solar and geomagnetic activity. Overall information about CHAMP, its STAR accelerometer, and mission profile in general are also available.

Sutton et al. [2005][25] contains additional information related to the derivation of atmospheric densities from the CHAMP satellite. Calibration of accelerometer bias and scale factors, including variation in time is made using available GPS data for the positioning of CHAMP. Winds in the thermosphere were assumed to have a negligible effect on perceived atmospheric density, and the accuracy of measurements from CHAMP was judged to be largely due to uncertainty in calibration, as well as neglected winds. In this study, time periods near three geomagnetic storms were examined and compared against results obtained from semi-empirical models to illustrate limitations within the models.

The accelerometer aboard the CHAMP satellite has been used to observe numerous solar and geomagnetic events, as well as their ability to cause significant density variations in the thermosphere these events were examined in Forbes et al. [2005][26], Sutton et al. [2005][25], Sutton et al. [2006][27],Bruinsma et al. [2006][28], Bruinsma and Forbes [2007][29] and Sutton et al. [2007][30].

The accelerometer aboard CHAMP is much better able to observe short term density variations than existing empirical and analytical models that lack the temporal resolution required to observe these events. The accelerometer measured rapid density variations generating density waves that propagate towards the poles arising from these storms. CHAMP and GRACE are uniquely suited to the task of identifying these variations' amplitude and span due to the presence of their accelerometers, and their near polar orbits, which allow the satellites opportunities to observe almost all latitudes of the atmosphere.

Tapley et al. [2007][31] detailed the methods through which atmospheric densities may be derived from the GRACE satellites. Densities derived from the GRACE satellites' accelerometers have similar properties and drawbacks to the accelerometer aboard the CHAMP spacecraft, but the satellites orbit at higher altitudes.

The STAR accelerometer aboard CHAMP has also been used to model moderate and large scale density variations in the thermosphere in Bruinsma and Forbes [2008][32]. Density variations often generate waves that originate at high latitudes and then progress to lower latitudes. Typically, these waves dissipate at mid-range latitudes, however, the waves tend to take longer to dissipate if geomagnetic activity is high, and solar flux is low. Zhou et al. [2009][33] used the STAR accelerometer to model corrections for the NRLMSISE model during geomagnetic storms.

More recently research examining on-board accelerometers has been conducted using the GOCE satellite. Zhang et al. [2014][34] examined lunar tide and geomagnetic activity variations, and their effects on space weather, while Häusler et al. [2014][35] used GOCE to better model daily variations in the thermosphere.

The CHAMP and GRACE satellites are invaluable tools for examining the nature of the Earth's atmosphere through the use of their accelerometers, and their availability of both GPS and

SLR data for the satellites. Unfortunately, these three satellites suffer from very poor spatial coverage as compared to DCA techniques which may have upwards of 700 satellites supplying data.

1.5.3 Additional Approaches

Use of GPS receivers, or SLR range observations to estimate non-conservative accelerations have been previously examined in several papers. One technique is to use the standard DCA approach to the limited number of satellites that have POE data available, and use these results to modify existing models as in Doornbos et al. [2005][36]. Calibrating atmospheric models to better match data from higher accuracy readings, such as those from POEs, will lead to significant increases in accuracy of orbit determination. The research aimed to use both high accuracy data, and highly available though less accurate data to create model corrections that have increases in both spatial and temporal resolution.

GPS accelerometry is an additional approach wherein GPS receiver data is used to estimate accelerations due to non-conservative forces and was used in van den IJssel et al. [2005][37], van den IJssel and Visser [2005][38] and van den IJssel and Visser [2007][39]. GPS accelerometry uses precision orbit data to derive forces experienced by the satellite via drag. These forces can then be used to determine atmospheric density. Via this method, temporal resolutions of 20 minutes can be obtained for CHAMP data in both the along-track and cross-track directions. With the launch of GRACE, a highly accurate model of the earth's gravitational field exists, and fulfils GPS accelerometry's need for such an accurate model. GPS accelerometry is most accurate in the along-track direction, which is where the bulk of non-conservative forces are experienced due to drag and station-keeping maneuvers. The technique lacks the precision of accelerometer readings, but several additional missions utilizing GPS receivers are planned, which will increase the data pool from which to pull observations, and increase the spatial resolution achievable.

Montenbruck et al. [2005][40] used both batch and Kalman filter techniques to examine accelerations experienced by the GRACE-B satellite. Both approaches are highly accurate, with a resolution of 5 cm with dual frequency data, and 10 cm with single frequency data. The primary point of this study was to determine differences between filter/smoother techniques, and batch techniques. The study found that the extended Kalman filter/smoother is less expensive computationally, while the batch least-squares estimator is smoother and more robust during data gaps.

Willis et al. [2005][41] used Doppler Orbitography and Radio positioning Integrated by Satellite (DORIS), as well as SLR data to examine density variations in the thermosphere during periods of enhanced geomagnetic activity. The study analyzed satellites at varied altitudes from the 800-900 km range, to the 1300-1400 km range. Significant errors were found to exist for the considered atmospheric models; these errors were greatly improved with more enhanced data processing. DORIS is yet another way of obtaining highly accurate satellite state vectors, and allows for formulation of corrections to atmospheric density models.

1.6 Recent Research on Atmospheric Density Model Corrections along Satellite Trajectories

Some of the initial results, as well as the research leading up to this research are detailed in McLaughlin and Bieber [2008][42], McLaughlin et al. [2008a][43], and McLaughlin et al. [2008b][44]. In McLaughlin and Bieber [2008][42], derived neutral densities were checked for consistency in overlap periods between data sets. The sets typically have a two hour overlap at the beginning and end of each set of measurements. In the overlap areas, density variations were at worst 10%. When compared to accelerometer data from CHAMP, the derived densities exhibited a similar range of errors as observed by McLaughlin et al. [2008a][43].

Hiatt (2009)[45] examined the viability of using optimal orbit determination processes to model atmospheric density during a range of geomagnetic and solar activity levels by comparing derived densities to accelerometer densities. The study spanned numerous time periods, and input variables such as density and ballistic coefficient half-life were varied to study their effects on estimated densities. The accuracy of varying the input parameters was measured using the cross-correlation between the derived densities and the accelerometer derived densities[45]. This provided a quantitative measure of which variant of input parameters yielded the best results. Hiatt [2009] and Lechtenberg [2010] examined optimal half-life combinations for various combinations of solar and geomagnetic activity, as well as the observability of density variations.[45,46] The research used precision orbit ephemeris (POE) data as observations in an optimal orbit determination scheme that estimated density and ballistic coefficient simultaneously. The density estimation was found to correlate quite well with densities found from the accelerometers onboard CHAMP and GRACE, but the temporal resolution of the density estimates was significantly worse than densities obtained from the accelerometers. Atmospheric density variations have also been examined in McLaughlin et al. [2011], who looked at the variability of drag coefficients and hence, atmospheric density values over the course of 5 years for a select group of spherical satellites.[47,48]

Previous work focused on finding values of ballistic coefficient and density half-lives that best corresponded to independent measurements of atmospheric density. Since both values are estimated simultaneously these optimal values are required for estimation of atmospheric density corrections to the existing models. The best set of density and ballistic coefficient correlation half-lives was found as 180 minutes for the density correlation half-life, and 1.8 minutes for the ballistic coefficient half-life with CIRA 1972 as a baseline density model by comparing POE derived densities to accelerometer derived densities for the CHAMP and GRACE satellites in Lechtenberg [2010], Fattig et al. [2010], and McLaughlin et al. [2010, 2011].[48,49,50,51]

McLaughlin et al. [2012] and Mysore Krishna [2012] examined different methods of integrating geomagnetic activity levels, expanded POE derived densities to include TerraSAR-X and ICESat, and examined how varying satellite cross-sectional areas affected atmospheric density estimation. [52,53] Several satellites were examined in depth, as well as the effect of given errors in atmospheric density on the orbit characteristics of given satellites.[54,55] This research will aim to better define density corrections for additional satellites, namely the ANDE series of satellites.

1.7 Gauss-Markov Process

A Gauss-Markov process is often used to resolve difficulties that arise from unmodeled or inaccurately modeled forces that may unexpectedly act on the spacecraft. A Gauss-Markov process is introduced to the data to compensate for these forces as a source of process noise. A Gauss-Markov process, as the name suggests, conforms to the properties of both a Gaussian, or normal, distribution, and a Markov process in that the probability density function is solely dependent on the observation immediately preceding it, and not upon any observations earlier than the one immediately preceding it. A more detailed explanation of Gauss-Markov processes is available in Tapley et al. [2004][56].

1.8 Estimating Density and Ballistic Coefficient Separately

In the course of dealing with satellite drag, atmospheric density and ballistic coefficient are directly related through the drag equation. Separation of the two variables is difficult in an orbit determination process due to the obvious difficulty of having one equation, and two unknowns. Wright [2003][57] and Wright and Woodburn [2004][58] propose a method of estimating both parameters in real time.

Before a viable manner in which to separate the ballistic coefficient and the atmospheric density was formulated, ballistic coefficient estimates tended to absorb errors in both the density and ballistic coefficient models. The method by which both are estimated simultaneously

involves the two variables having markedly differing half-lives applied using a Gauss-Markov process. These exponential half-lives instruct the process to what degree it should consider previous measurements when inputting process noise. The analysis software used in this research, the Orbit Determination Tool Kit (ODTK), allows the user to manipulate both half-lives, which allows the user to examine the effectiveness of varying those two parameters. More information on this can be found in Wright [2003][57].

McLaughlin et al. [2009][59] examined nominal ballistic coefficients for the CHAMP satellite, as well as the effects of induced errors in filter initialization of the ballistic coefficient on atmospheric density estimation. More recently, extraction of drag coefficient values has been done using Direct Simulation Monte Carlo Methods (DSMC) by Mehta et al. [2013][60] who developed a parameterized drag coefficient model (PDMC) for the GRACE satellite that significantly reduced drag coefficient estimation errors. This method does tend to be rather computationally intensive though.

1.9 Examined Satellites

1.9.1 CHAMP

The CHAMP satellite, as seen in Figure 1.1 was launched on July 15, 2000 with a scheduled mission life of 5 years to generate highly precise gravity and magnetic field measurements[61]. CHAMP was specifically designed to measure the medium wavelength gravity field, map Earth's global magnetic field, and perform atmosphere/ionosphere sounding. The CHAMP satellite possesses the highly accurate Spatial Triaxial Accelerometer for Research (STAR) instrument, which was used in this study to determine atmospheric density[61].

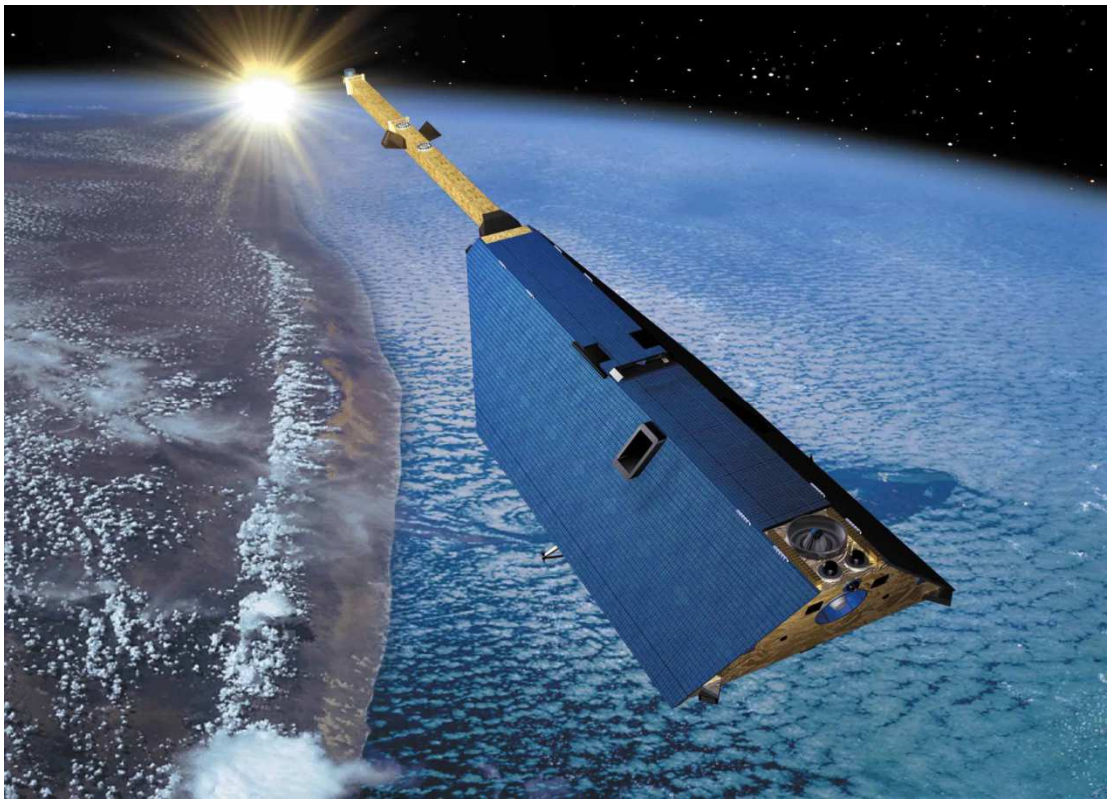

Figure 1.1: Artist Rendering of the CHAMP Satellite in Orbit[62]

1.9.2 GRACE

The GRACE project, as seen in Figure 1.2 is a small network of two satellites designed to measure the Earth's gravity field very precisely. To accomplish this goal, both satellites are also equipped with very sensitive accelerometers, as well as an inter-satellite ranging system that allows the satellites to measure very small perturbations in the distance between them[63]. The perturbations arise when one of the satellites passes over a region of the Earth that is more or less dense than the Earth as a whole, causing that satellite to either accelerate or decelerate and alter the distance between them[63]. The accelerometers aboard these two spacecraft were used to analyze corrected densities found in this research.

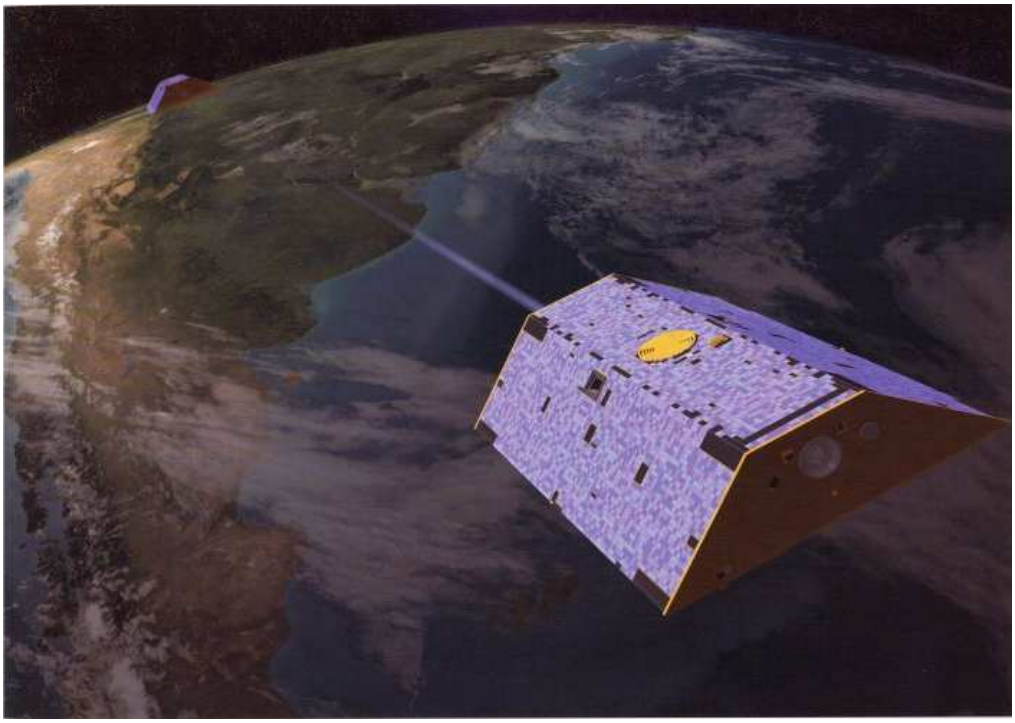

Figure 1.2: Artist Rendering of the GRACE Satellites in Orbit[63]

1.9.3 ANDE

ANDE RR

The ANDE satellites were designed as low-cost methods of monitoring thermospheric neutral density at low altitudes of 400-350 km and below.[64,65] The ANDE satellites are paired into sets of two. The first ANDE mission, which later evolved into the ANDE-RR mission, consisted of two spherical satellites with differing masses. The first, the Mock ANDE Active (MAA) had a mass of around 50 kg, while the Fence Calibration (FCal) satellite had a mass nearer to 75 kg[64]. In future places in this work, the MAA satellite may be referred to as RRa, and the FCal as RRp, denoting their active and passive natures respectively. The two satellites had slightly different diameters, and also had different surfaces from one another. MAA's outer sphere was made from anodized aluminum, and was an inch and a half wider than FCal at 19 inches in diameter, while the FCal satellite's outer sphere was made from nickel plated brass[64]. Both satellites possess 30 retro reflectors for generating range data using the International Laser Ranging Service (ILRS) [64].

Figure 1.3: ANDERR-MAA (left) and ANDERR-FCal (right)

ANDE-2

The intermediate mission, ANDE-2, had an active satellite (Castor) and a passive satellite (Pollux). The two are identical size and shape, but have purposefully different masses so that the satellites would separate as non-conservative forces acted on them during the course of their lifespan. Castor being almost 20 kg heavier than the lighter Pollux. As the satellites separate, they were intended to provide researchers with an opportunity to study small-scale variations in atmospheric density through the measurement of the drag forces acting on the spacecraft. The active satellite has a wind and temperature spectrometer, as well as a GPS receiver.[66] Both satellites possess 30 retro reflectors for generating range data using the International Laser Ranging Service (ILRS).[67] The ANDE satellites are also intended to be used as calibration satellites for modelling atmospheric density.[68]

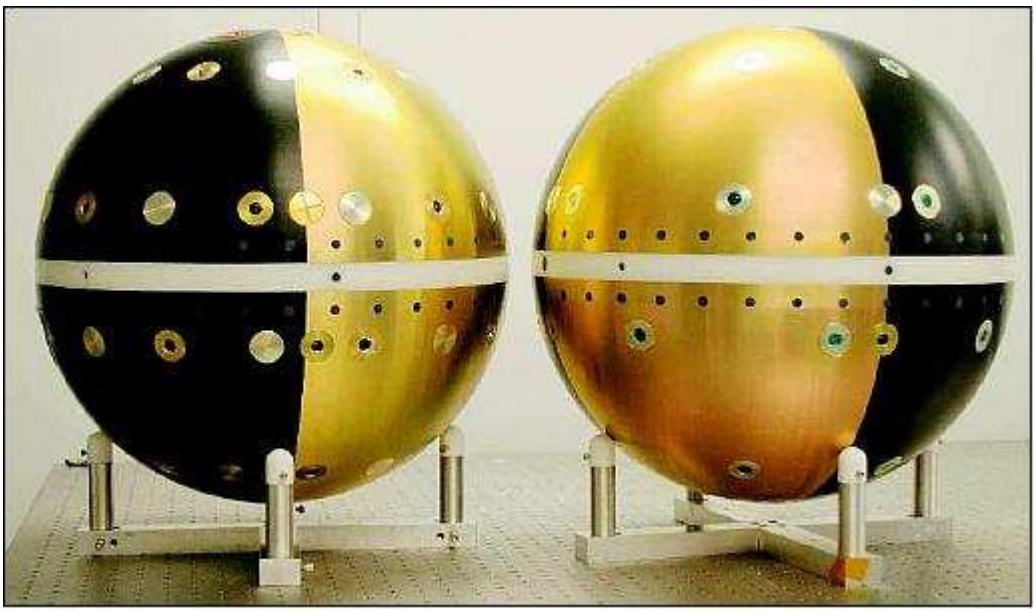

Figure 1.4: ANDE-2 Spheres, Castor (Left) and Pollux (Right)

SPINSAT

In late 2014, the Special Purpose Inexpensive Satellite (SPINSAT) satellite was launched with the mission to provide a test bed for an electrically controlled solid propellant system. SPINSAT's secondary mission, however, was to provide a calibrated means by which to examine atmospheric density at higher solar activity levels than were examined by the ANDE and ANDE-2 missions, which flew primarily during solar minimum. SPINSAT houses 68 retroreflectors, is .558m in diameter, has a mass of 57 kg, and is spherical in shape, making it an excellent candidate for estimating atmospheric density corrections.[69]

Figure 1.5: SPINSAT soon after Deployment

1.9.4 Examined Satellite Summaries

This section includes pertinent details of the examined satellites, such as lifespan, initial ballistic coefficient or drag coefficient, mass, and initial altitude. Since ballistic coefficient and drag coefficient are inherently related, the derived value is listed in parentheses. Ballistic coefficient is estimated as part of the filter/smoother process, and is defined in ODTK for CHAMP as having a nominal value of 0.00444 m^2/kg, and for GRACE as 0.00687 m^2/kg, though these ballistic coefficients change over time, and are adjusted accordingly.[70] Since ODTK will estimate BC at the same time as atmospheric density, the remaining satellites had initial estimates of drag coefficient input as estimated from Walker et al. [2014][71] using their analysis of drag coefficient of sphere's dependence on solar activity levels.

Table 2: Satellite Characteristic Summary

Satellite	Launch Date	Reentry Date	Mass (kg)	Cross-Sectional Area (m^2)	Initial C_D	Ballistic Coefficient (m^2/kg)	Altitude (km)	Inclination (°)
CHAMP	Jul. 15, 2000	Sep. 19, 2010	519.3	0.742500	(3.1)	0.00444	~400	87
GRACE-A	Mar. 17, 2002	---	481.3	0.950000	(3.48)	.00687	~485	89
ANDErra	Dec. 21, 2006	Dec. 25, 2007	52.0	0.182921	2.05	(0.00720578)	~350	51.6
ANDErrp	Dec. 21, 2006	May 25, 2008	62.7	0.155179	2.05	(0.00507364)	~350	51.6
ANDE-2c	Jul. 30, 2009	Aug. 18, 2010	47.5	0.182921	2.05	(0.00790282)	~350	51.6
ANDE-2p	Jul. 30, 2009	Mar. 28, 2010	27.4	0.182921	2.05	(0.01366480)	~350	51.6
SPINSAT	Sep. 21, 2014	---	57.0	0.244845	2.1	(0.00902059)	~400	51.6

1.10 Progression of Unique Research

Previous research focused primarily on POE data, and how it could optimally be used to estimate atmospheric densities, as well as examined the limitations of the approach. Current research uses what was learned in previous research to expand the precision orbit determination approach to examining density to a wider array of satellites that have available SLR data and fairly easily characterized drag characteristics. In particular, the ANDE family of satellites are examined as satellites from which to make corrections to existing atmospheric models, taking advantage of their simple geometry. Jacchia-Bowman is examined using these techniques, whereas in the past it has not been. A much broader range of altitudes can be examined by applying these techniques to additional satellites. This will give better spatial resolution with which to eventually integrate density into an assimilative atmospheric density model.

2 Methodology

This section details the methods used to obtain results for determining the atmospheric density in the thermosphere. Position and velocity vectors were derived from Precision Orbit Ephemerides (POE) for the CHAMP and GRACE satellites in an optimal determination process. For other satellites, processed SLR data were used as measurements in an optimal determination process. The optimal orbit determination process yielded density values along the path of the satellite, as well as ballistic coefficient values for the satellite during that time. Various baseline density models were examined to demonstrate differences in how baseline density models are accounted for when making corrections to atmospheric neutral density. Techniques for the analysis of POE data are detailed in Hiatt [2009][45] and Lechtenberg [2010] [46].

2.1 Satellite Laser Ranging

Density estimation results were derived from processed Satellite Laser Range (SLR) data for the ANDE Castor satellite in an orbit determination process. The orbit determination process yielded density values along the path of the satellite, as well as ballistic coefficient values for the satellite during that time. Range data are currently available for all of the ANDE family of satellites in the form of .npt data and .crd data from the International Laser Ranging Service (ILRS) ftp website. Both of these data types are normal point data for the satellite in question, but with slightly different formatting. Full rate data is also available, as well as processed position data available that are useful for orbit initialization as .nrl files which give predicted positions in Cartesian coordinates.

In this research, processed range data were used as measurements in the optimal orbit determination scheme. These data provided measurements for use as input for a Kalman filter/smoother scheme using Gauss-Markov processes.

2.2 Satellite Laser Ranging Residuals

Measurement residuals for SLR measurements give context to estimated atmospheric density in illustrating how accurate the measurements are for a given satellite, and how closely the predicted satellite state matches those given measurements. If residuals are too large, the measurements lose meaning, and any atmospheric density approximations derived from them are inaccurate and suspect. For the ANDE-Castor satellite, some measurement arcs had outliers that skewed average residuals to higher values, though those arcs later converged to lower values this may have been due to a discontinuity in data, or to inaccurate initial satellite state conditions that caused predictions to diverge from actual measurements.

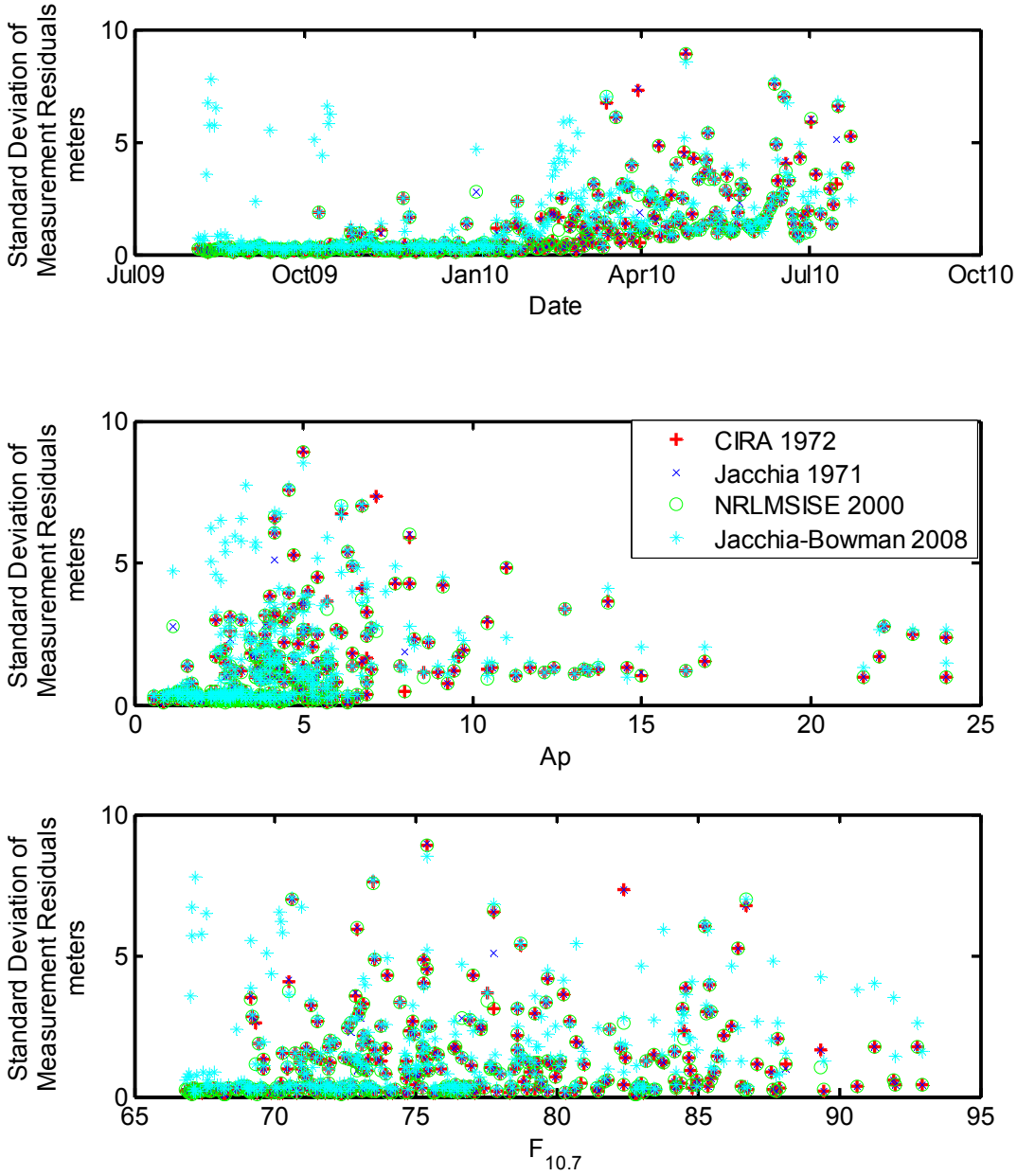

Figure 2.1: ANDEc RMS Residuals for Individual Arcs

The measurement residuals seen in Figure 2.1 show a slow trend towards increasing residuals as the satellite neared the end of its life, as altitude decreased until reentry. In general,

the root mean squared (RMS) residuals for any given satellite arc, are likely to be between .2 and 1 meter.

2.3 Precision Orbit Ephemerides

POE data are currently available for both the CHAMP and GRACE satellites in the form of Precision Science Orbits (PSO) or Rapid Science Orbits (RSO). This data is available from Helmholtz Centre Potsdam at their website at http://isdc.gfz-potsdam.de. Processing and accuracy details of RSOs can be found in Konig et al. [2002][72], Michalak et al. [2003][73], Konig et al. [2005][74], and Konig et al. [2006][75]. Accuracies for RSOs vary from 5-10 cm for most of the mission lives of the satellites, though early in the mission lives, accuracies were as poor as 25 cm. There is no published data for the accuracies of PSOs, though, as PSOs incorporate additional gravity field solutions obtained from CHAMP, these solutions are assumed at least as accurate, and likely more accurate than RSOs. For this reason, PSO data is preferred over RSO data when available. PSO data is unavailable for dates prior to 2003 and after 2005, and none are available for the GRACE or TerraSAR-X satellites.

2.4 Optimal Orbit Determination

An optimal orbit determination scheme is used to determine atmospheric densities in the thermosphere. The process for utilizing an optimal orbit determination scheme is detailed in Tapley et al. [2004][56], with additional information available in Vallado [2007]1 and Montenbruck and Gill [2001][76].

Orbit determination is the process of estimating orbits in relation to the central body provided accurate measurements are available. Orbiting bodies can be affected by several forces, predominately geopotential, and third-body gravitational accelerations, as well as forces due to pressures acting on the surface areas of the satellites. Artificial satellites tend to have increased sensitivity to pressure effects such as drag, solar radiation pressure (SRP), and Earth albedo. This

is due to the decreased density of artificial satellites as opposed to natural satellites which are generally solid throughout.

Each measurement used in an orbit determination is preferred to possess sufficient orbit parameters to predict the future state of the satellite. This requires that at least six independent elements of the state be known. In Cartesian coordinates, these are the position and velocity vectors; in Keplerian elements, these are eccentricity (*e*), semimajor axis (a), inclination (i), right ascension of the ascending node (Ω), argument of periapsis (ω), and either mean anomaly (M) or true anomaly (ν)[56]. The general state at time *t* is denoted as $\mathbf{X}(t)$, and the orbit determination problem can be stated as: If at an initial time t_0, the state $\mathbf{X}_0$ of a satellite following a ballistic trajectory is known, then equations of motion can be integrated to give the state of the vehicle at any time[56]. Unfortunately, the initial state of the orbiting body is not precisely known, and the dynamical models are also not precisely known. This causes the path of the orbiting body to deviate from the predicted path. For this reason, updated measurements are required for better approximating the true trajectory of the orbiting body, though the trajectory cannot be precisely known due to random and systematic errors. Measurements are generally in the form of range, range-rate, azimuth, elevation, and other observable quantities that often must be used to determine more useful state variables, as these measurements are often nonlinear functions of the desired state variables[56].

In this research, as well as the research leading up to it, POE data were used as measurements in the optimal orbit determination scheme. These POEs provided relatively accurate measurements for use as input for a Kalman filter/smoother scheme using Gauss-Markov processes, both of these concepts will be described in greater detail later in this section.

There is ongoing debate over the "best" method to determine orbit characteristics. Some methods compile results more quickly, though at the risk of reduced accuracy. Some methods are

able to take into account observations as they are transmitted to ground, while others require all measurements to be accumulated.

According to Wright [2002][77] any orbit determination scheme may be referred to as optimal if the following criteria are met:

1. *"Sequential processing is used to account for force modeling errors and measurement information in the time order in which they are realized.*
2. *The optimal state error estimate* $\Delta\hat{X}$ *is the expectation of the state error* ΔX *given the measurement residual* Δy. *That is:* $\Delta\hat{X} = E\{\Delta X \mid \Delta y\}$. *This is Sherman's Theorem.*
3. *Linearization of state estimate time transition and state to measurement representation is local in time, not global.*
4. *The state estimate structure is complete.*
5. *All state estimate models and state estimate error model approximations are derived from appropriate force modeling physics, and measurement sensor performance.*
6. *All measurement models and measurement error model approximations are derived from appropriate sensor hardware definition and associated physics, and measurement sensor performance.*
7. *Necessary conditions for real data:*
    - *Measurement residuals approximate Gaussian white noise.*
    - *McReynolds' filter-smoother consistency test is satisfied with probability 0.99.*
8. *Sufficient conditions for simulated data: The state estimate errors agree with the state estimate error covariance function.*

The first six requirements defined standards for optimal algorithm design, and the creation of a realistic state estimate error covariance function. The last two requirements enable validation: They define realizable test criteria for optimality. The last requirement implies the development and use of a physically realistic measurement simulator."

2.5 Gauss-Markov Process Half-Lives

Gauss-Markov processes are introduced into the orbit determination scheme in ODTK through the use of the density and ballistic coefficient correlation half-lives. These half-lives are expressed as ratios of the corrections as compared to the calculated values using the CIRA 1972 model in the form of $\Delta\rho/\rho$ and $\Delta B/B$, which represent the amount of time required for the estimated correction to the corresponding values to decay to half its original value[78].

The ODTK help file[78] details how these variables are incorporated into Gauss-Markov processes. To examine this, let a random scalar variable be denoted by $x=x(t_k)$, in this case, that random scalar variable is either density or ballistic coefficient. The variable satisfies the equation:

$$x(t_{k+1}) = \Phi(t_{k+1}, t_k)\, x(t_k) + \sqrt{1-\Phi^2(t_{k+1}, t_k)}\, w(t_k) \tag{0.9}$$

where $w(t)$ is a Gaussian variable with a fixed standard deviation and a zero mean. Since $w(t)$ in this equation is solely dependent on the previous measurement, the $w(t)$ process is also Markovian. The initial value of the Gauss-Markov process is equal to the initial value of the scalar variable being examined, and the transfer function is defined as:

$$\Phi(t_{k+1}, t_k) = e^{\alpha|t_{k+1}-t_k|} \tag{0.9}$$

where

$$\alpha = \frac{\ln(.5)}{\tau} \tag{0.9}$$

and τ is the user supplied half-life for the given variable[78].

2.6 Filter-Smoother Description

For the ANDE-2 Castor satellite, processed SLR data are used as measurements in a sequential filtering scheme, while precision orbit ephemerides were input as measurements into a sequential filtering scheme for the CHAMP and GRACE satellites that estimates a series of state variables including position and velocity vectors, density corrections, spacecraft ballistic coefficient corrections, as well as other variables of interest such as station biases, additional forces, measurements, and model parameters. The filter process takes previous measurements into account to integrate force models and determine the future state of orbiting bodies. The filter outputs a converged state and covariance estimate that are later used in the following iterations of the filter approach.

The smoother process takes the last output of the filtering process and works sequentially backwards to the initialization state of the filter. The smoother's output is determined by inputting the series of outputs from the filtering scheme. None of the initial measurements used in the determination of the filter solutions are used for the smoother process. The smoother is applied to take into account all measurements that are included in the files[56]. Detailed explanations and algorithms for filter and smoother schemes can be found predominately in Tapley et al. [2004][56], with supplemental information in Vallado [2007]1, Montenbruck and Gill [2001][70], Wright [2002][77], and Bowman et al. [2008][79].

2.7 McReynolds' Filter-Smoother Consistency Test

The McReynolds's Filter-Smoother consistency test is used to test the validity of the filter and smoother state estimations by comparing them to one another. The test consists as follows; a dimensionless ratio, $\vec{R}$, is formed from the difference between the smoother and filter values compared to the square root of the difference between the two covariance matrices. The test is gauged as passed if 99% or more of the ratios are less than 3.

$$R = \left| \frac{\vec{X}_{i,filter} - \vec{X}_{i,smoother}}{\sigma_i} \right| \leq 3 \tag{0.9}$$

$$\sigma_i = \sqrt{\overline{P}_{i,filter} - \overline{P}_{i,smoother}} \tag{0.9}$$

The McReynolds's consistency test is further detailed in Wright [2002][77].

2.8 Using Orbit Determination to Estimate Atmospheric Density

The orbits estimated using ODTK are optimal in the least-squares, or minimum variance sense. ODTK's sequential filtering scheme estimates corrections to baseline atmospheric density models and ballistic coefficients for the satellites, calculates residuals, conducts position and velocity consistency tests, generates state variables, and estimates other state parameters of interest. A smoother was then applied to the filtered data in order to take into account all measurements in the determination of these parameters and increase the accuracy of the estimations. The filter/smoother scheme estimates atmospheric density corrections, and ballistic coefficient corrections, including covariance matrices determined by the physics models associated with the orbit determination scheme. ODTK is able to estimate corrections to a variety of baseline atmospheric density models, including Jacchia-1971, CIRA-1972, Jacchia-Roberts,

MSISE-1990, NRLMSISE-2000 models, and Jacchia-Bowman 2008. ODTK used the GRACE Gravity Model GGM02C to integrate the equations of motion for the satellite, which is complete to the 200th degree and order, and incorporates GRACE satellite data, as well as terrestrial gravity information[79]. ODTK also includes additional force models in addition to drag, these models include a complex assessment of the Earth's gravity field, solar, Earth infrared, and Earth albedo radiation pressure, lunar and solar gravitational effects, general relativity, and ocean and solid Earth tides.

Results for estimating the atmospheric density clump into two groups divided by baseline atmospheric density model. The first group consists of the Jacchia-1971, Jacchia-Roberts, CIRA-1972, and Jacchia-Bowman models due to the models being based on the original Jacchia-1970 model with accumulated improvements over the years. The second grouping consists of the MSISE-1990 and NRLMSISE-2000 models which are both Mass Spectrometer Incoherent Scatter Extended models.

There are two corrections to atmospheric density that are applied in ODTK, the first takes place as a global correction to density based upon the daily $F_{10.7}$ value, the daily A_p value, and the height of perigee of the satellite orbit. These corrections are then propagated through the orbit through the use of exponential Gauss-Markov processes; a transformation is applied to relate the current corrections for atmospheric density to the corrections determined at perigee. The second correction is used to account for each sequential observation of the satellite, as well as more up to date information of current atmospheric conditions. The sequential process allows for corrections to be estimated as each observation is acquired. These sequential measurements take into account the user provided density and ballistic coefficient exponential Gauss-Markov process half-lives.

2.8.1 Varying Baseline Density Model

Four baseline models are examined to illustrate differences between the models. The Jacchia-1971 model was examined as it is a robust model that has endured for many years and is the basis for many subsequent models. The CIRA-1972 model was examined due to the model's exemplary results in predicting atmospheric neutral density in this orbit determination scheme during examination in previous work.[42,43,44,45,46] The NRLMSISE model was examined as it possesses a different root for the analysis of neutral atmospheric densities from the Jacchia derived models. The Jacchia-Bowman 2008 model was examined as the model has recently become more available, and has not been examined in this context before. More detailed descriptions of these models can be found in Section 1.4.

2.8.2 Solar and Geomagnetic Activity Level Bins

The results of the examination of the accuracy and precision of the model densities as compared to corrected densities are sorted into divisions defined in Section 1.4.1 in Table 1. This is done to examine how the atmospheric neutral density deviations from model baselines are affected by the varying degrees of geomagnetic and solar activity.

2.9 Validation of the Estimated Atmospheric Density

The densities derived in ODTK for CHAMP and GRACE were compared to those derived from CHAMP and GRACE accelerometers by Sean Bruinsma of CNES. The accelerometer derived densities were averaged over 10 second intervals as described in Bruinsma and Biancale [2003][22] and Bruinsma et al. [2004][24]. These results were detailed in Lechtenberg[46], and were used to determine an optimal combination of density half-life (180 Minutes) and ballistic coefficient half-life (1.8 Minutes), for examined satellite arcs.

3 Results

Two sets of results will be presented, the first is a comparison of using two different baseline atmospheric density models and their effect on atmospheric density estimates for the path of the ANDE Castor satellite, and the second are density variations for satellites that have an independent method of measuring density through accelerometers, as well as density variations for the ANDE satellite. These satellites are the CHAMP and GRACE-A satellites respectively. The data span examined for the satellites was during a three month period in late 2009 specifically August through October. During this period all three examined satellites were active and were thus experiencing the same levels of solar and geomagnetic activity. During the time period examined, there was little variation in solar and geomagnetic activity levels with low to moderate levels of solar activity and quiet levels of geomagnetic activity.

3.1 Derived Atmospheric Density Values for ANDE

Presented here are atmospheric density values for the ANDE Castor satellite during its orbits on August 17, 2009, on that date, the mean A_p value was 2 corresponding to quiet geomagnetic conditions, and the daily 10.7 cm solar flux ($F_{10.7}$) was 68.1 corresponding to low solar activity. Low levels of both solar and geomagnetic activity persisted throughout the lifespan of ANDE, which existed entirely within a protracted solar minimum that saw historically low levels of both types of activity.

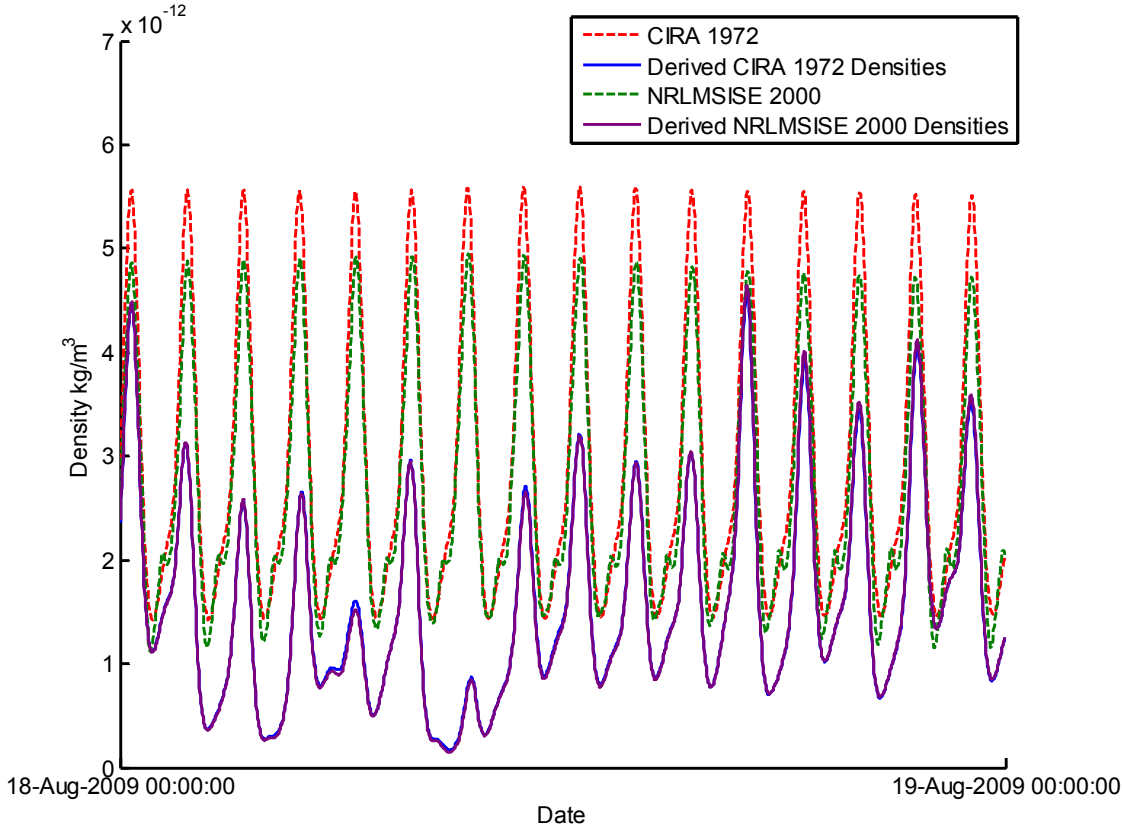

Figure 3.1: ANDE Density Values on August 18, 2009

For the ANDE satellite during the given conditions in Figure 3.1, both models are quite regular, with consistent maximums and minimums. For the time periods examined, the model density values for both the CIRA 1972 model and the NRLMSISE model are similar. The estimated densities are consistently less than the model densities. Given the similarities between both models estimated densities and previous research revealing that the Jacchia based models tend to better estimate atmospheric density, the NRLMSISE densities are omitted from following figures. The densities' similarities are likely due to the extraordinarily quiet nature of the time period, or the ANDE satellites' low altitude, or a combination of the two. Current atmospheric density models also appear to under-estimate atmospheric neutral density for this time period as well.

3.2 Derived Atmospheric Density Values for Multiple Satellites

Presented here are atmospheric density values for the GRACE-A, CHAMP, and ANDE satellites during the same time periods. The first time span examined is the day prior to Figure 3.1, August 17, 2009. On this date, solar activity was low, and the geomagnetic activity was quiet. The second time span is a few weeks after the first on the date of September 13, 2009, and the third is another few weeks after that on October 6, 2009. For both of the latter two time-spans, solar activity levels were low and the Earth was geomagnetically quiet as well. The time period ANDE-2 was active happened to be during solar minimum, and the solar and geomagnetic activity levels were low/quiet, respectively, throughout the examined time period of August-October. During these time periods, both the CHAMP and ANDEc satellites were at around 330 km in altitude, while the GRACE-A satellite was at an altitude of 474 km.

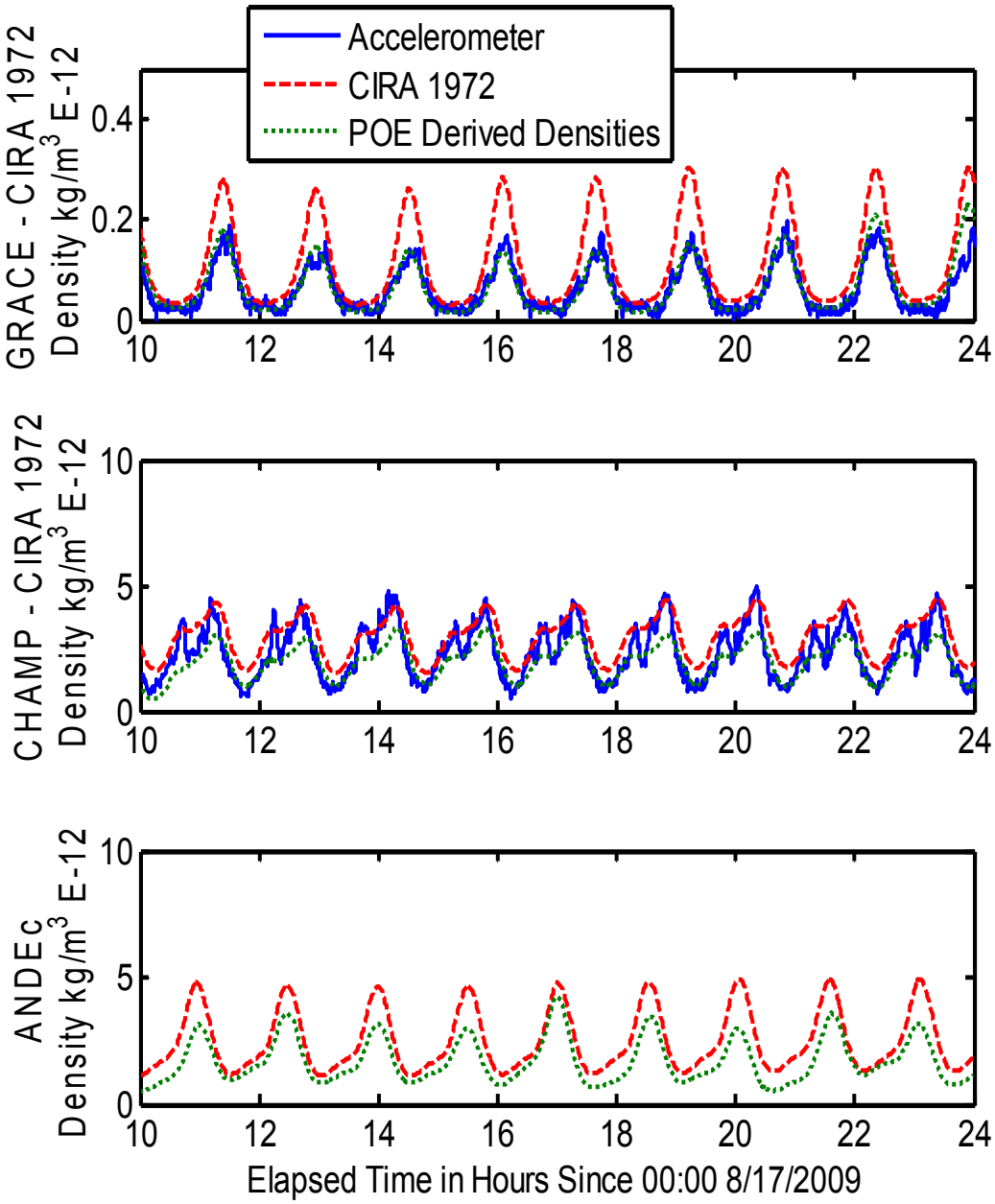

Figure 3.2: Orbit Derived, Accelerometer Derived, and Predicted Density Values for GRACE, CHAMP, and ANDE on August 17, 2009

In Figure 3.2, all three satellites show more variable density values than predicted by current atmospheric density models. For the GRACE satellite, density values are consistently over-estimated, while for CHAMP, the density values for both the baseline model densities and the estimated densities are quite close to measured values, though the baseline model densities are consistently higher than the estimated ones. The model densities show overestimation of atmospheric densities for all three satellites.

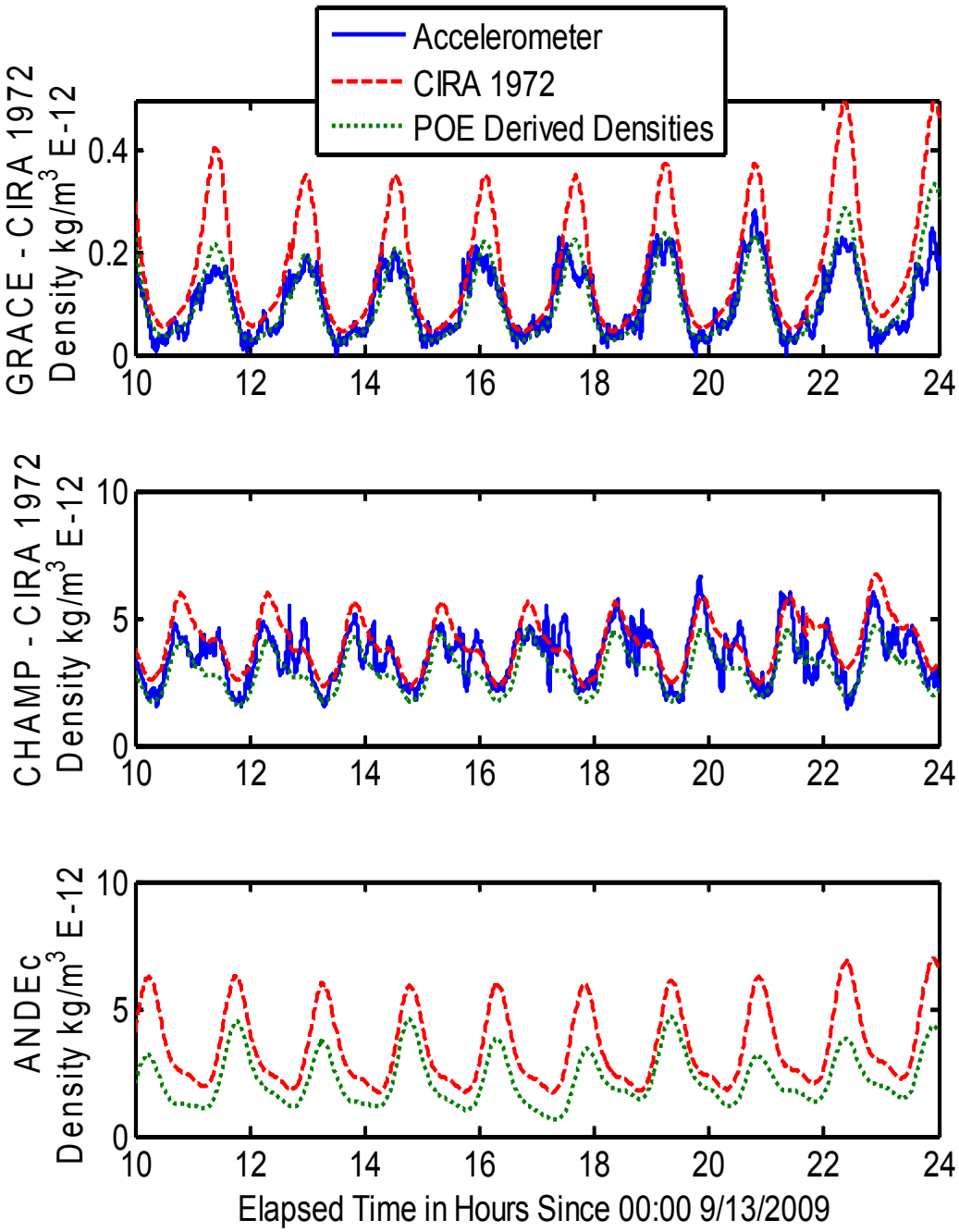

Figure 3.3: Orbit Derived, Accelerometer Derived, and Predicted Density Values for GRACE, CHAMP, and ANDE on September 13, 2009

Figure 3.3 shows the different density values for the GRACE, CHAMP and ANDE satellites on September 13, 2009. Again, model densities at all three satellite's altitudes are over-estimated, with densities at the CHAMP satellite's altitude being more in line with accelerometer derived values, with the estimated densities showing improvement over the baseline model.

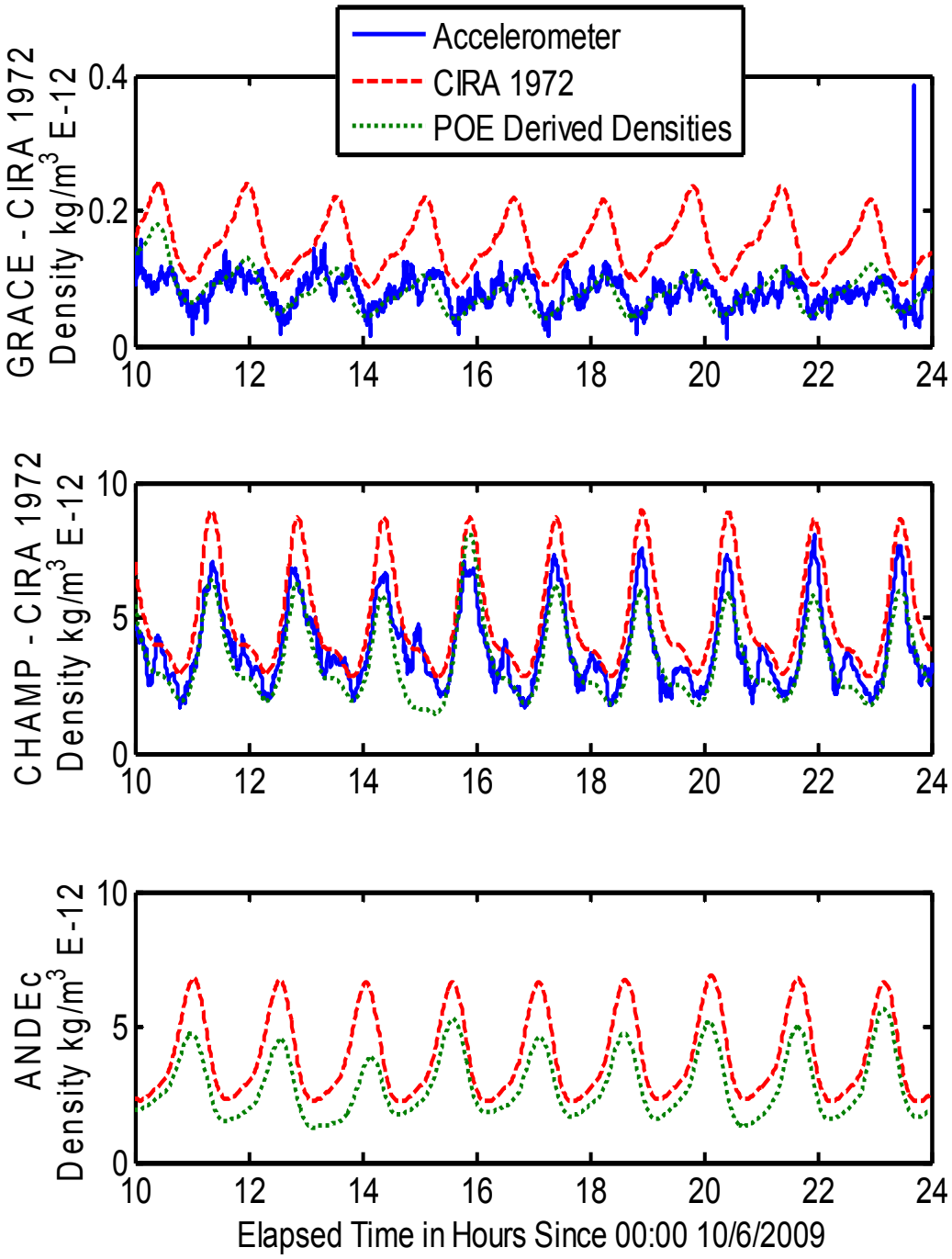

Figure 3.4: Orbit Derived, Accelerometer Derived, and Predicted Density Values for GRACE, CHAMP, and ANDE on October 6, 2009

In Figure 3.4, density values are presented for October 6, 2009 for all three satellites again. Consistent with both previous figures, all three satellites, CHAMP, GRACE, and ANDEc show regularly overestimated density values. Similar to the previous figures, the baseline density model significantly overestimates the estimated densities, and results for the ANDEc satellite are consistent with results for the CHAMP and GRACE satellites.

3.3 ANDEc Analysis for Different Baseline Density Models

ANDEc operated during quiet periods of solar and geomagnetic activity, extremely low in fact. There were no periods of activity above moderate for both solar and geomagnetic activity for the lifespan of the ANDE Castor satellite.

The data has been binned into daily, weekly and monthly (30 day) data periods and graphed with dependence on date, geomagnetic activity levels, and solar activity levels. Both the density correction factor, (Mean Estimated rho/Mean model Rho), and non-biased standard deviation (UBSTD) which was adjusted for these density correction factors, were examined.

$$DFC = \frac{\bar{\rho}_{Estimated}}{\bar{\rho}_{Model}}$$

$$UBSTD = \sqrt{\frac{1}{N}\left(x_{i_{Estimated}} - DFC \times x_{i_{Model}}\right)^2}$$

3.3.1 Daily ANDE-C Density Dependence

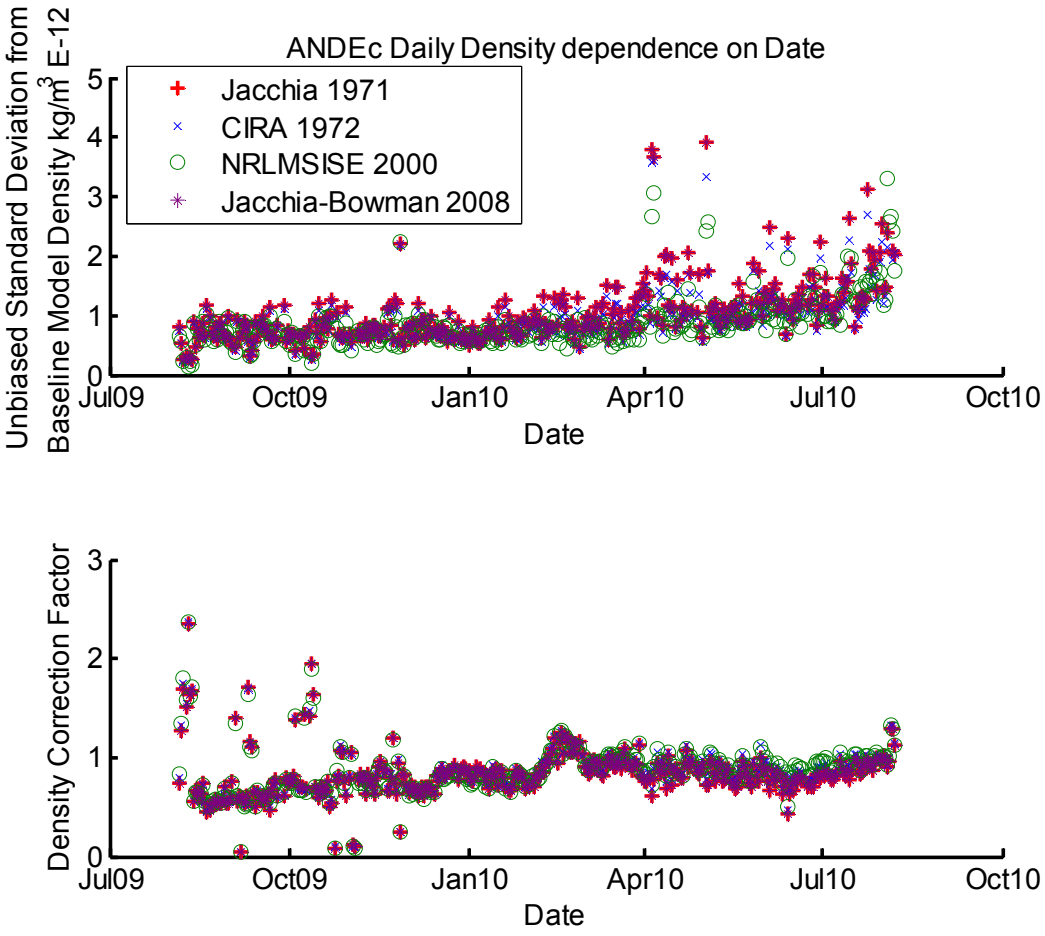

Figure 3.5: ANDEc Daily Density Dependence on Date

In Figure 3.5, there is but one trend in dependence on date, and that is that both the density correction factor, and the unbiased standard deviation, get notably worse around late July in 2010, and into August of 2010, this is due to the rapidly decaying orbit of the Castor satellite, which re-entered the Earth's atmosphere on August 18, 2010. There are a few other outliers as well earlier in the time span, likely due to inaccurate initial conditions, which led to a rejection of subsequent observations, and a radical increase in perceived errors in atmospheric density.

Throughout the lifespan of ANDEc, atmospheric models typically overestimated the atmospheric density as seen in most of the density correction factor values being less than one.

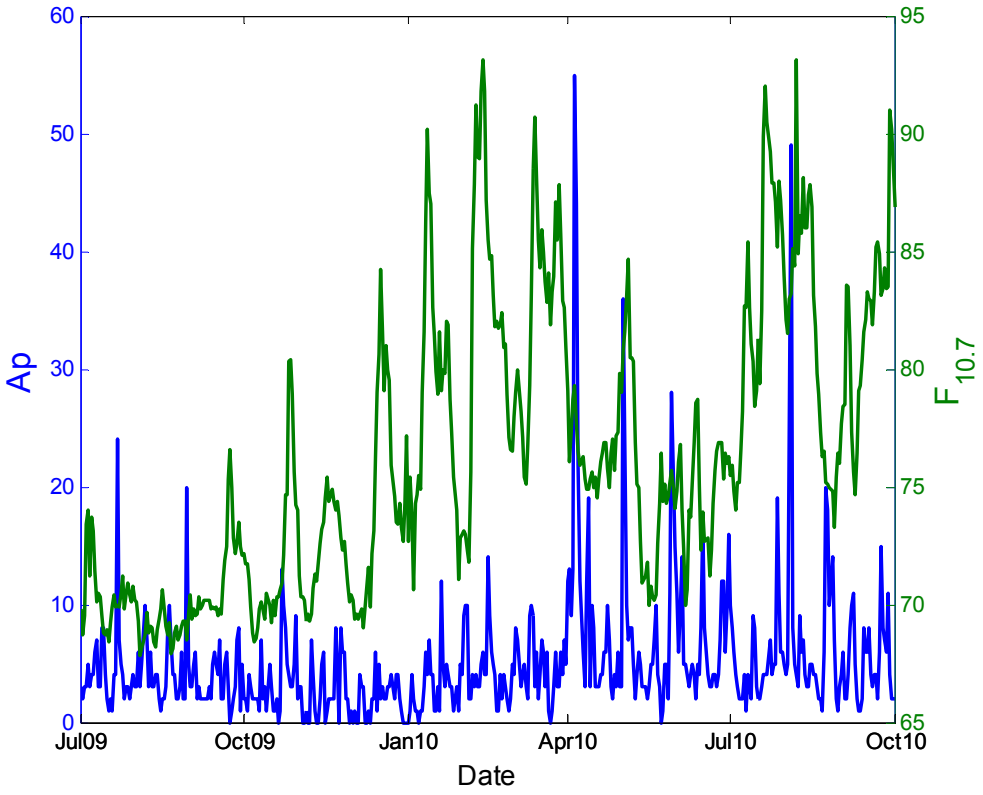

Figure 3.6: Solar and Geomagnetic Activity Levels during the Lifespan of ANDEc

In Figure 3.6, solar and geomagnetic activity levels are shown for the entire life of the ANDEc satellite. There is a period between January and April in 2010 during which there is significantly higher solar activity, which corresponds to a slight increase in density correction factor around the same time.

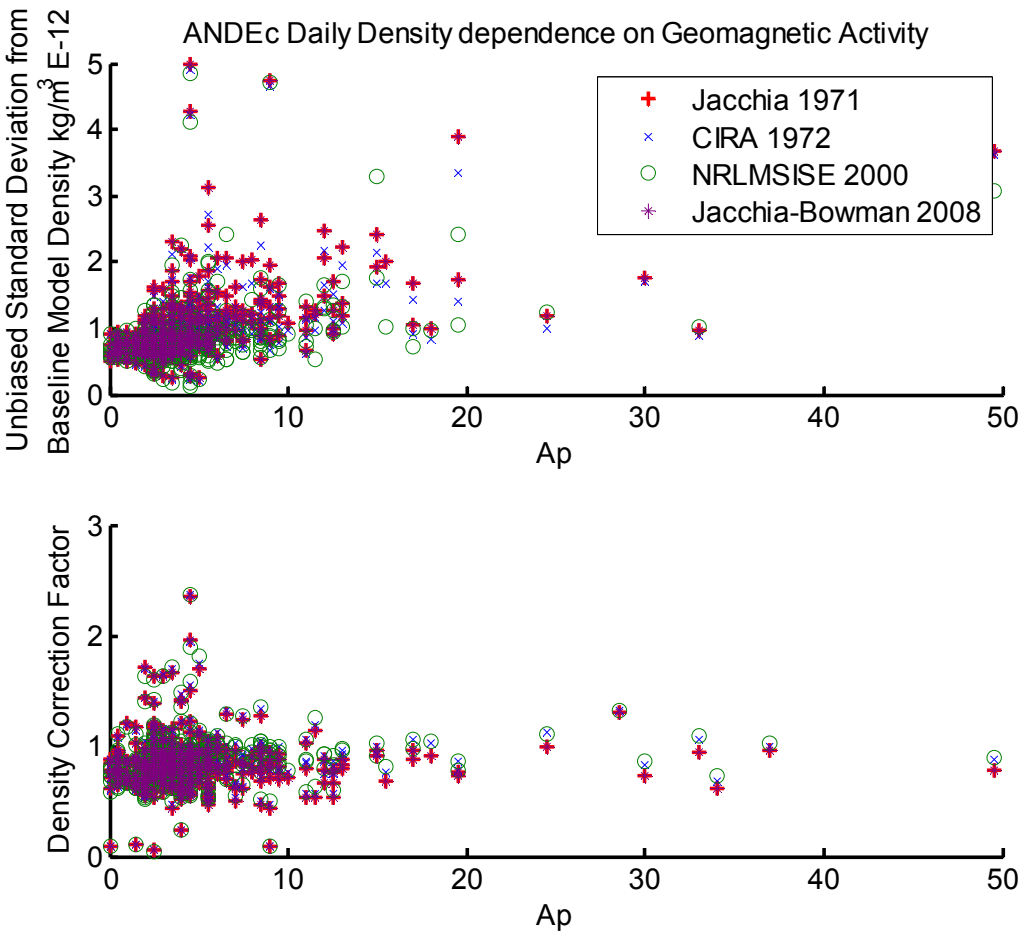

Figure 3.7: ANDEc Daily Density Dependence on Geomagnetic Activity

In Figure 3.7, there is little apparent impact of geomagnetic activity on the density correction factor. Though there is a noticeable upward trend in unbiased standard deviation as geomagnetic activity increases, at least on a daily basis.

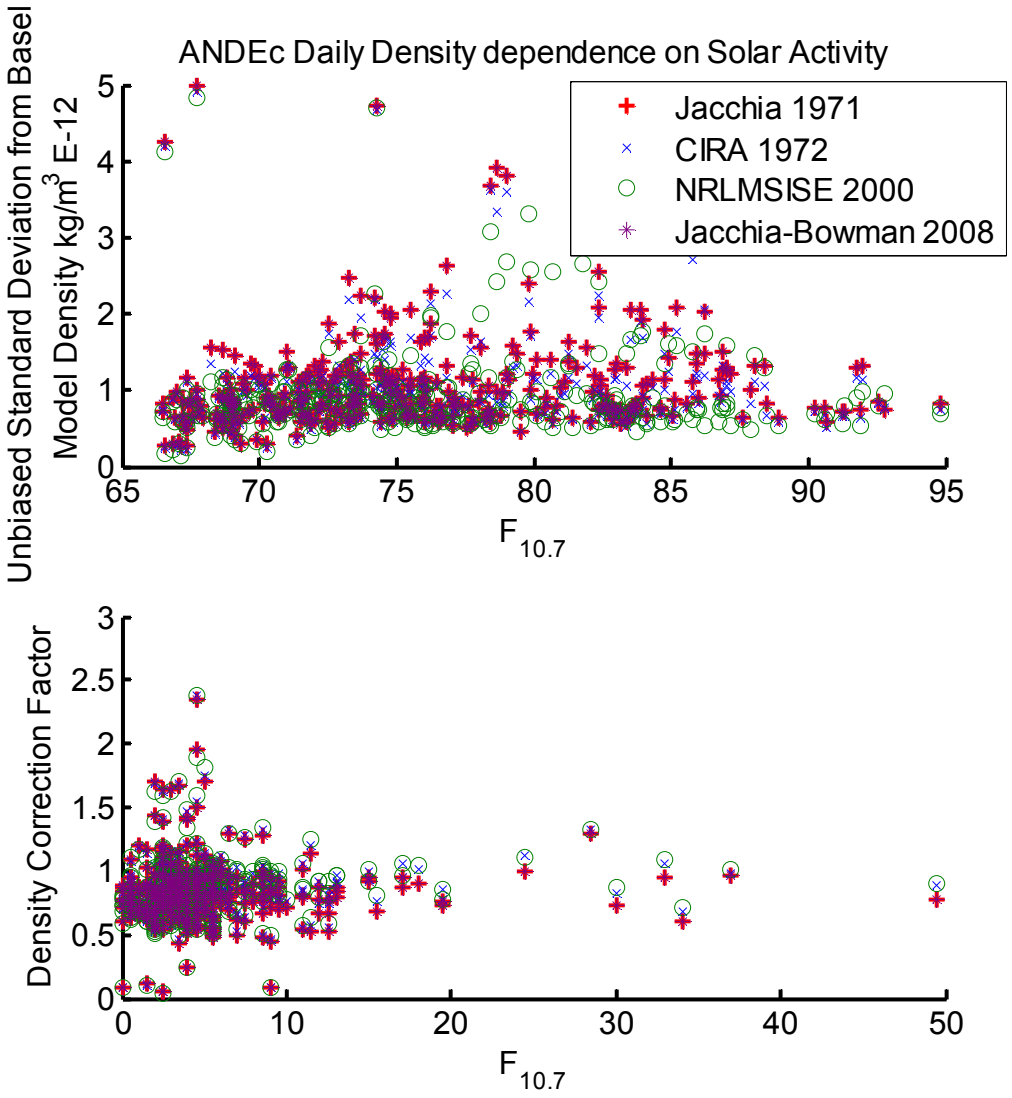

Figure 3.8: ANDEc Daily Density Dependence on Solar Activity

In Figure 3.8, solar activity levels appear to have little to no impact on the density correction factor, or the unbiased standard deviation. At persistently low levels of both solar and geomagnetic activity, geomagnetic activity appears to be the primary driver of errors incurred in density estimation.

3.3.2 Weekly ANDE-C Density Dependence

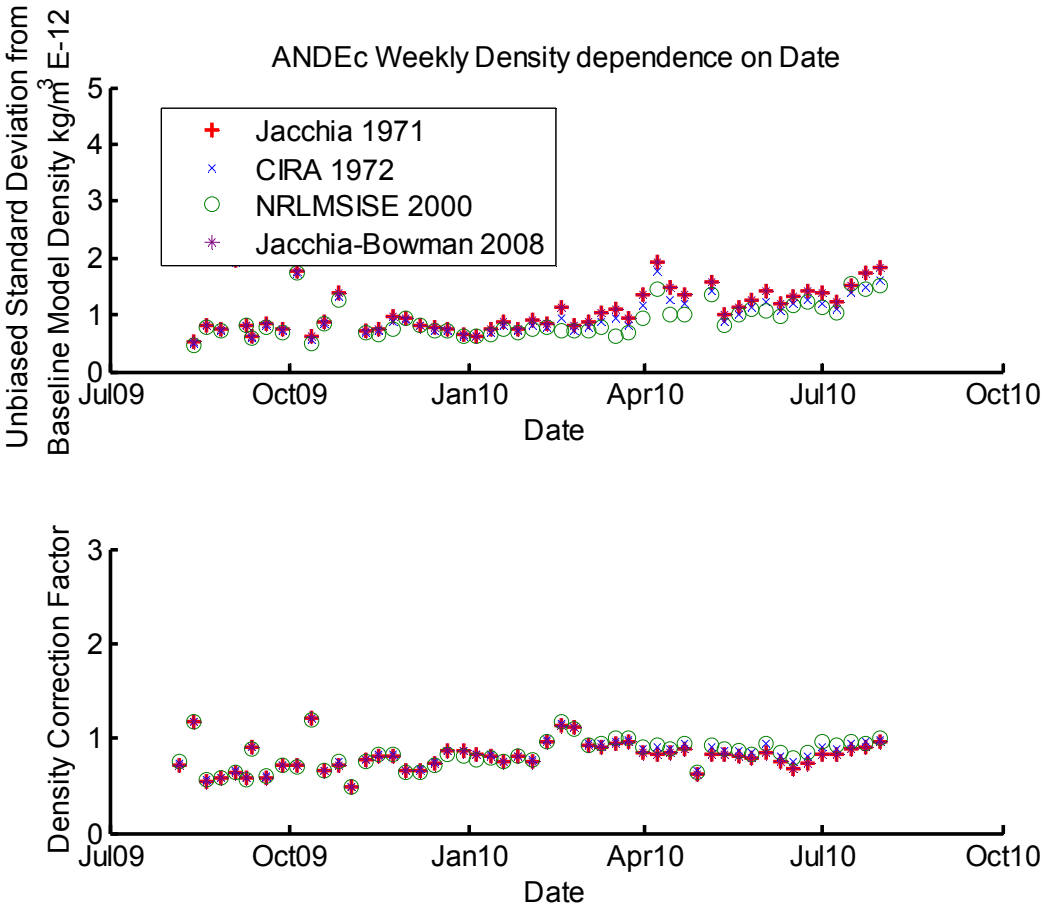

Figure 3.9: ANDEc Weekly Density Dependence on Date

In Figure 3.9, the data was binned on a weekly basis, and shows similar trends to the data examined for daily data, with increasing errors incurred near the end of the satellite's life span.

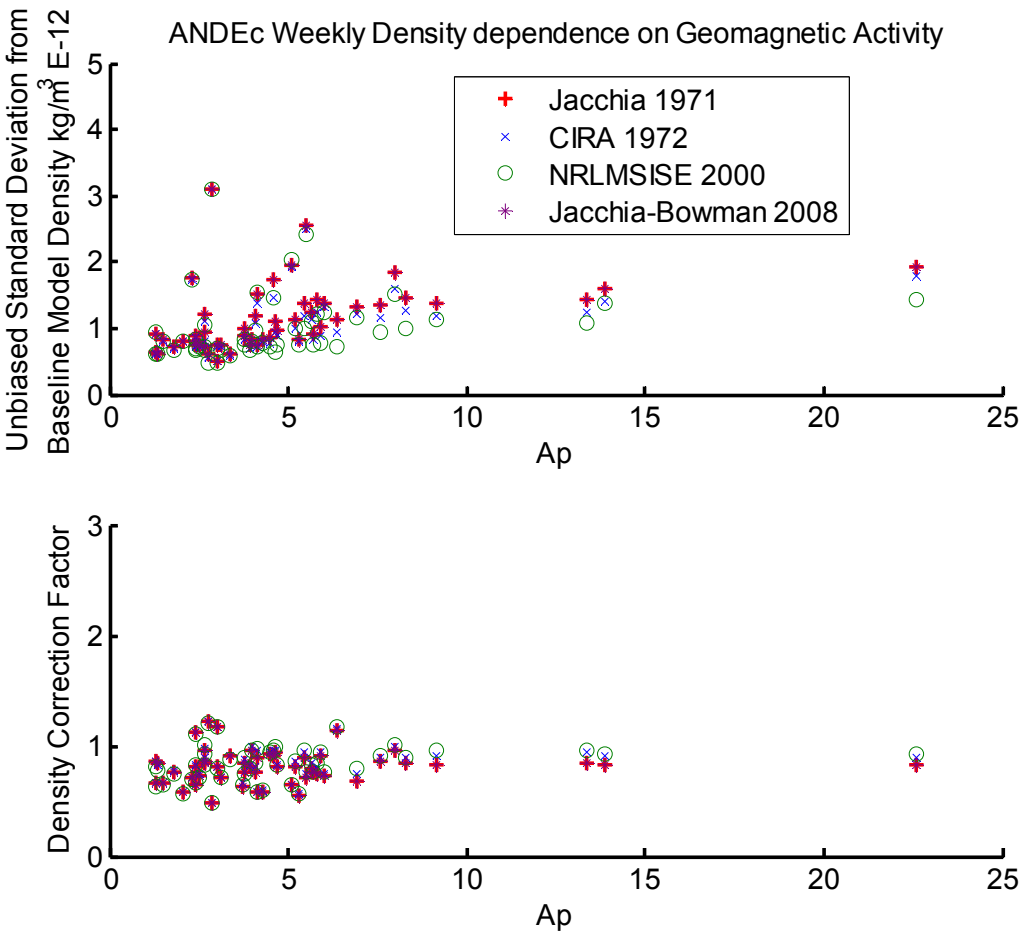

Figure 3.10: ANDEc Weekly Density Dependence on Geomagnetic Activity

In Figure 3.10, similar results to those of Figure 3.7 are seen with what appears to be an almost linear relationship between unbiased standard deviation and geomagnetic activity.

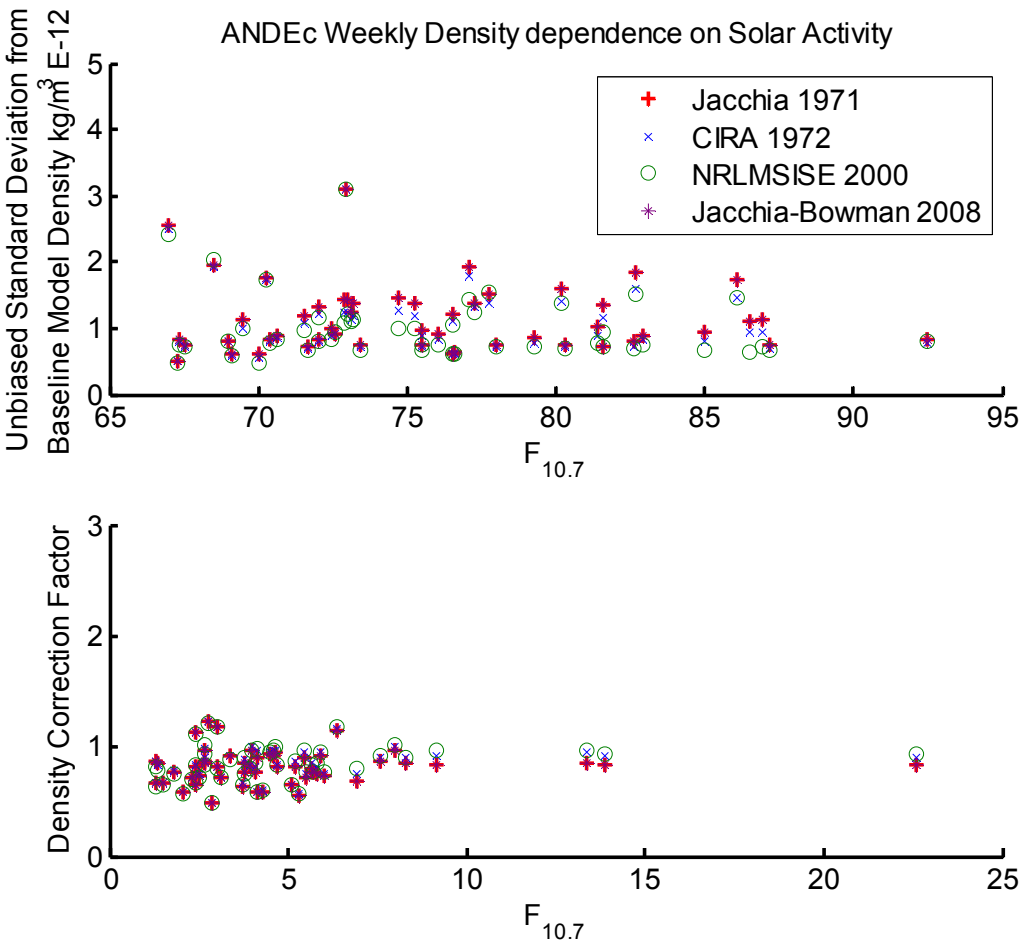

Figure 3.11: ANDEc Weekly Density Dependence on Solar Activity

In Figure 3.11, no additional trends or dependence on solar activity are clarified by the binning of data into weekly data sets.

3.3.3 Monthly ANDE-C Density Dependence

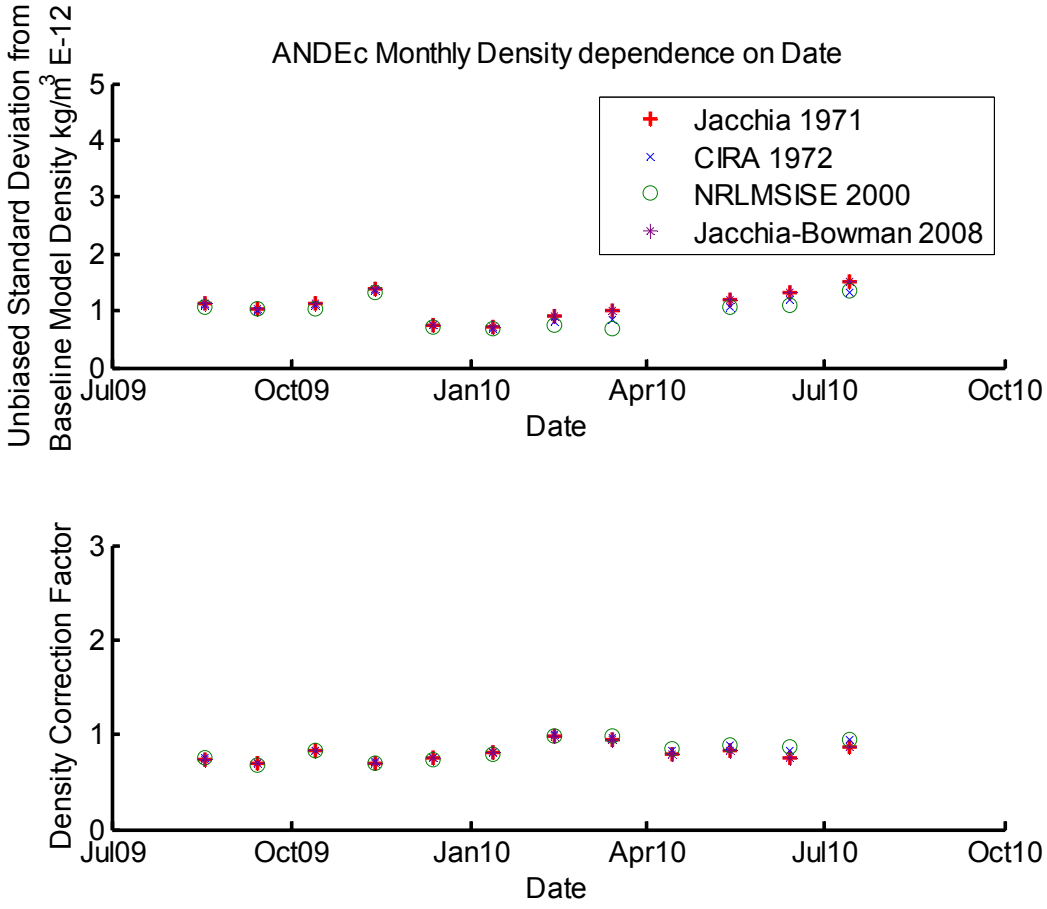

Figure 3.12: ANDEc Monthly Density Dependence on Date

In Figure 3.12, any useful trends are completely obscured due to the large size of the data bins, demonstrating the futility of attempting to examine the data on this timescale, particularly for a satellite life span of just over a year.

3.3.4 Solar and Geomagnetic Activity Effects

Density correction factor and non-biased RMS were also examined for geomagnetic and solar activity bins. There were no data points during the lifespan of the satellite for active geomagnetic conditions, or for any solar activity levels higher than moderate, and thus those activity levels are excluded from the following tables.

Table 3: ANDEc Non-Biased Standard Deviation dependence on Geomagnetic Activity in kg/m^3 E-12

Geomagnetic Activity Level	CIRA 1972	Jacchia 1970	NRLMSISE 2000	Jacchia-Bowman 2008
Quiet	1.082	1.052	1.033	1.009
Moderate	0.980	0.919	0.887	0.949

In Table 3, the non-biased standard deviations actually decrease and the models are more precise as geomagnetic activity increases from quiet levels to moderate levels. In addition, all of the models perform with similar results.

Table 4: ANDEc Density Correction Factor dependence on Geomagnetic Activity

Geomagnetic Activity Level	CIRA 1972	Jacchia 1970	NRLMSISE 2000	Jacchia-Bowman 2008
Quiet	0.750	0.755	0.745	0.914
Moderate	0.533	0.567	0.601	0.648

Although Table 3 shows increased precision with increasing geomagnetic activity, Table 4 shows that current atmospheric models actually are less accurate, and yield values closer to estimated densities at quiet geomagnetic levels.

Table 5: ANDEc Non-Biased Standard Deviation dependence on Solar Activity in kg/m^3 E-12

Solar Activity Level	CIRA 1972	Jacchia 1970	NRLMSISE 2000	Jacchia-Bowman 2008
Low	1.112	1.084	1.073	1.032
Moderate	0.970	0.932	0.887	0.926

Table 5 shows similar results as Table 3 except that atmospheric density predictions are increasing in precision with respect to solar activity as opposed to geomagnetic activity.

Table 6: ANDEc Density Correction Factor dependence on Solar Activity

Solar Activity Level	CIRA 1972	Jacchia 1970	NRLMSISE 2000	Jacchia-Bowman 2008
Low	0.726	0.731	0.724	0.903
Moderate	0.812	0.821	0.803	0.929

Table 6, shows that the accuracy of the atmospheric density models actually increases with solar activity, with the Jacchia-Bowman model performing better than the remaining three models. This is likely due to the unprecedented extended solar minimum that was undergone during the satellites' lifespans. None of the models included data from these extremely quiet conditions, with the possible exception of the Jacchia-Bowman 2008 model.

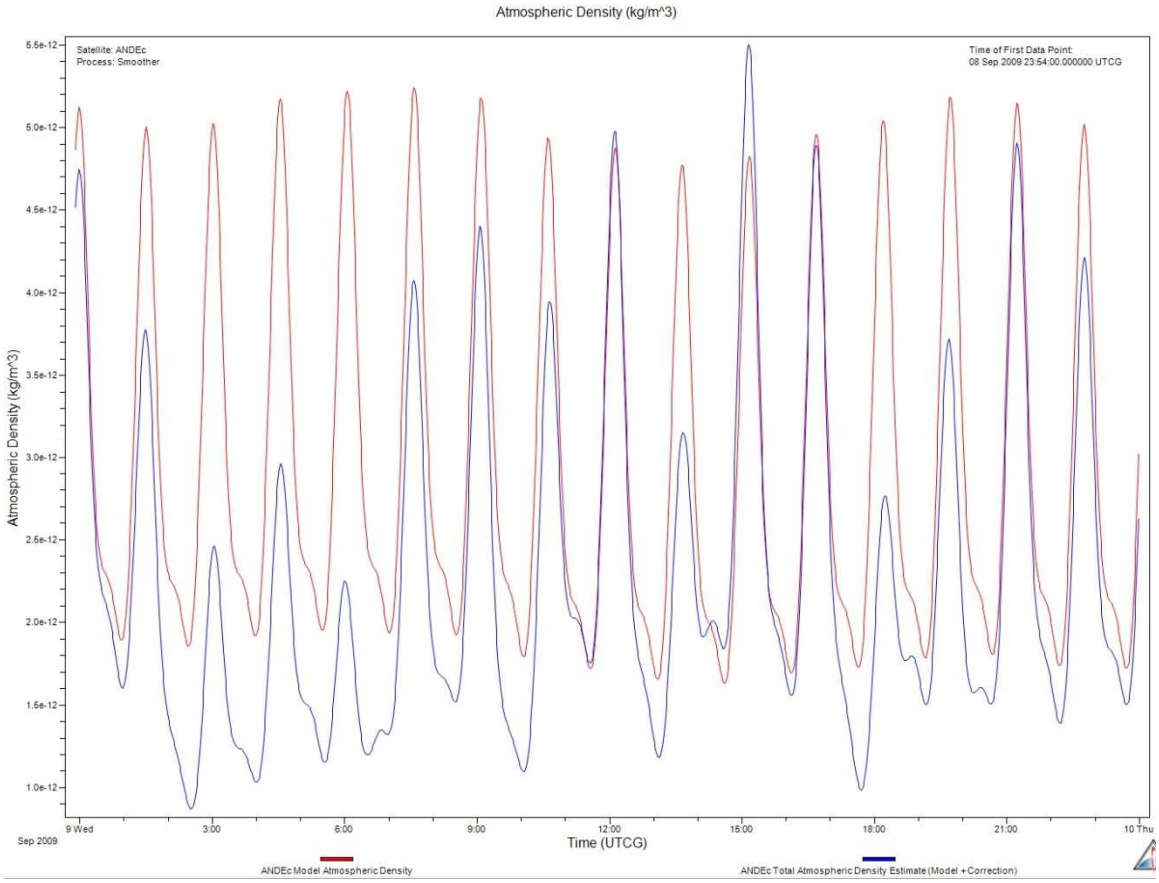

Figure 3.13: Example of Dissimilarity between CIRA 1972 Model Density Values, and Total Density Values Determined from Measurements for ANDEc on September 9, 2009

Due to the extreme similarity in results between three of the density models, CIRA 1972, Jacchia 1970, and Jacchia-Bowman 2008, in Table 3 through Table 6, density values were re-examined for a few sample arcs to verify that density values were in fact changing with baseline model. In Figure 3.13, the estimated and predicted densities are wildly dissimilar. This dissimilarity causes the model to be unable to project short term corrections, as the bulk of the corrections are focused on the larger scale dissimilarity. Since the three models share a similar background, it is logical that they are similar as they all apply similar corrections to density values to match the data. The models vary mostly in the short term formulations, but these are

rendered near unobservable by the fact that the models must make a large adjustment as a baseline.

3.4 Covariance Dependence for ANDE Satellites

As with all estimated quantities, there is a measure of uncertainty associated with the derived density values for any satellite. In this section the dependence of these uncertainty values on satellite, altitude, and both geomagnetic and solar activity.

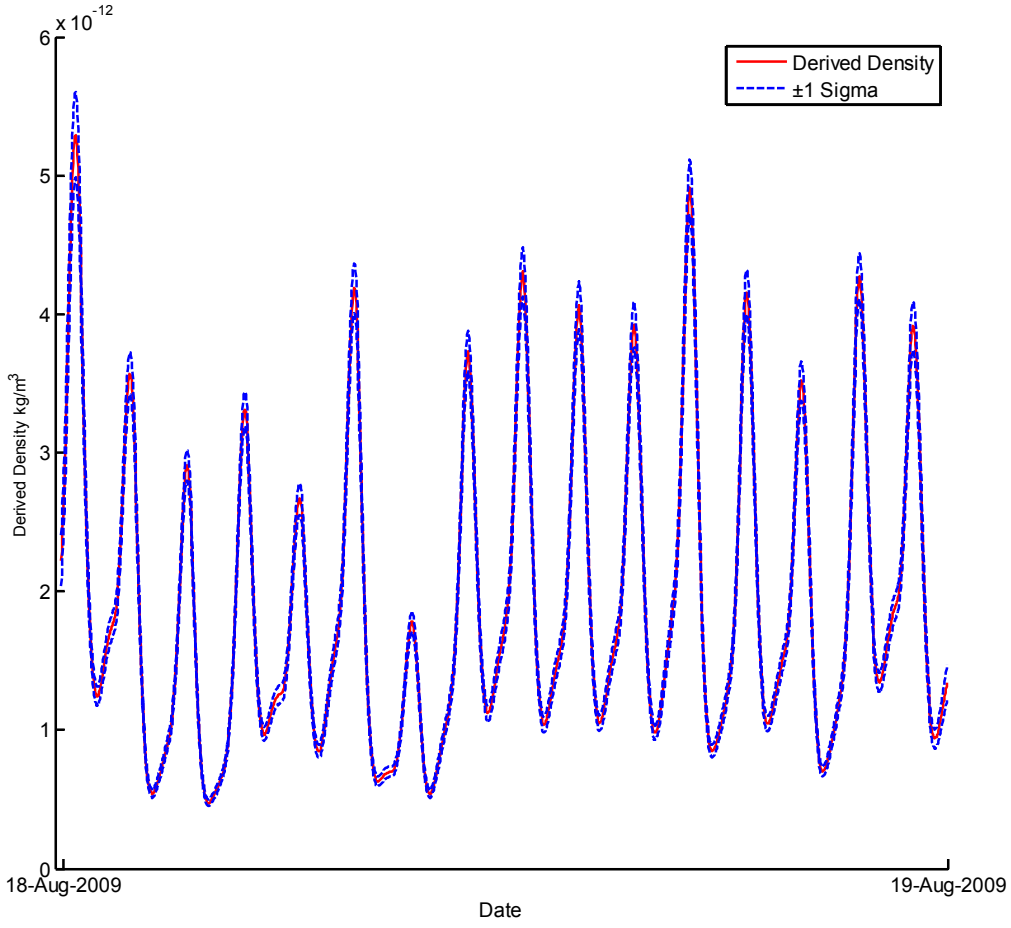

Figure 3.14: Derived Densities and Sigma Values for ANDEc on August 18, 2009

In Figure 3.14 density and density sigma values are given for the ANDE Castor satellite, the uncertainty associated with the density values is seen most prominently in the maxima and minima during the orbits of the satellite. The uncertainty values are also slightly larger as a percentage of the derived densities at the beginning and end of the arc.

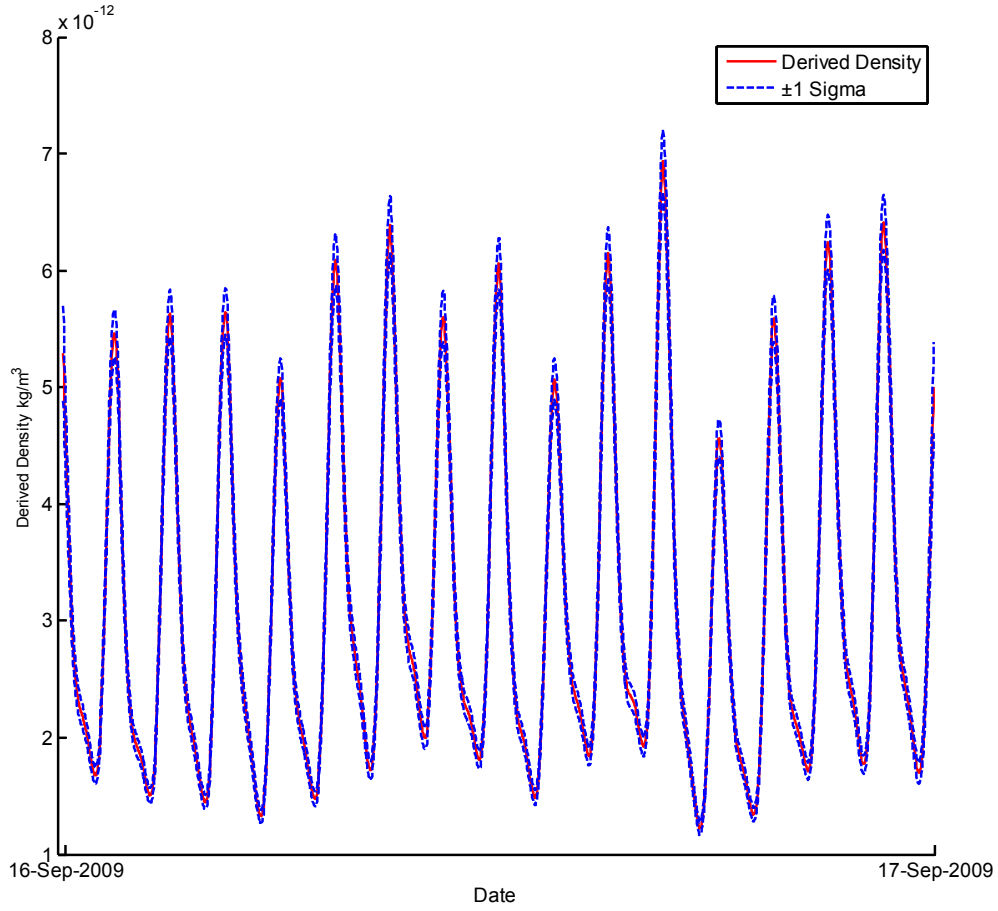

Figure 3.15: Derived Densities and Sigma Values for ANDEp on September 16, 2009

In Figure 3.15 density and density sigma values are given for the ANDE Pollux satellite, the uncertainty associated with the density values is seen most prominently in the maxima and minima during the orbits of the satellite. The values are extremely similar to those seen for the Castor satellite previously with the uncertainty values being slightly larger as a percentage of the derived densities at the beginning and end of the arc.

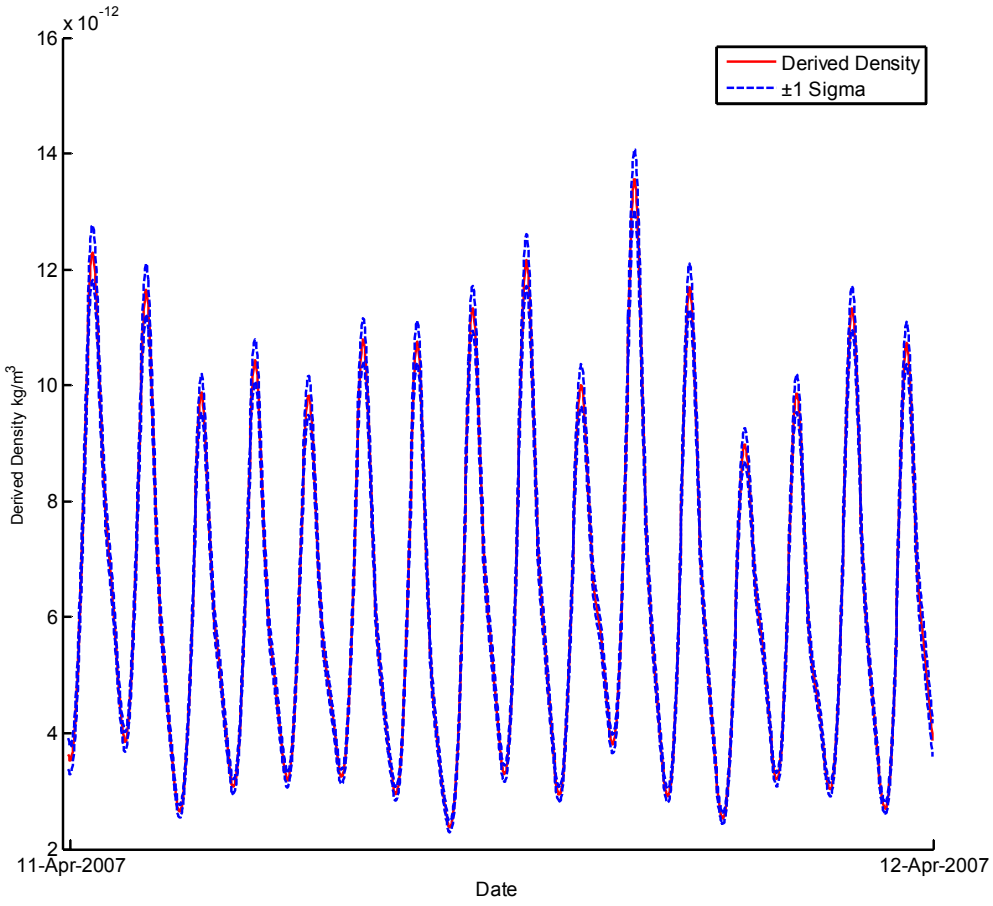

Figure 3.16: Derived Densities and Sigma Values for ANDErra on April 11, 2007

In Figure 3.16 density and density sigma values are given for the ANDE Risk Reduction Active satellite, the uncertainty associated with the density values is seen most prominently in the maxima and minima during the orbits of the satellite. The values are extremely similar to those seen for the previous ANDE satellites with the uncertainty values being slightly larger as a percentage of the derived densities at the beginning and end of the arc.

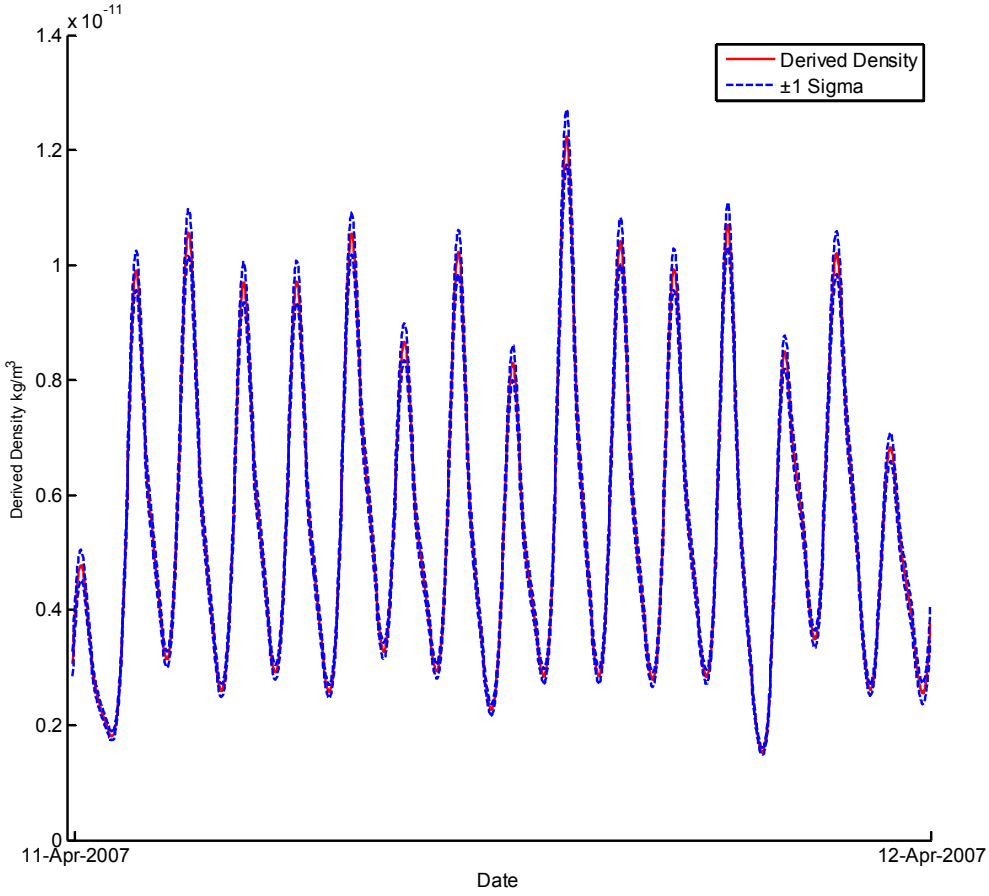

Figure 3.17: Derived Densities and Sigma Values for ANDErrp on April 11, 2007

In Figure 3.17 density and density sigma values are given for the ANDE Risk Reduction Passive satellite, the uncertainty associated with the density values is seen most prominently in the maxima and minima during the orbits of the satellite. The values are extremely similar to those seen for the previous ANDE satellites with the uncertainty values being slightly larger as a percentage of the derived densities at the beginning and end of the arc.

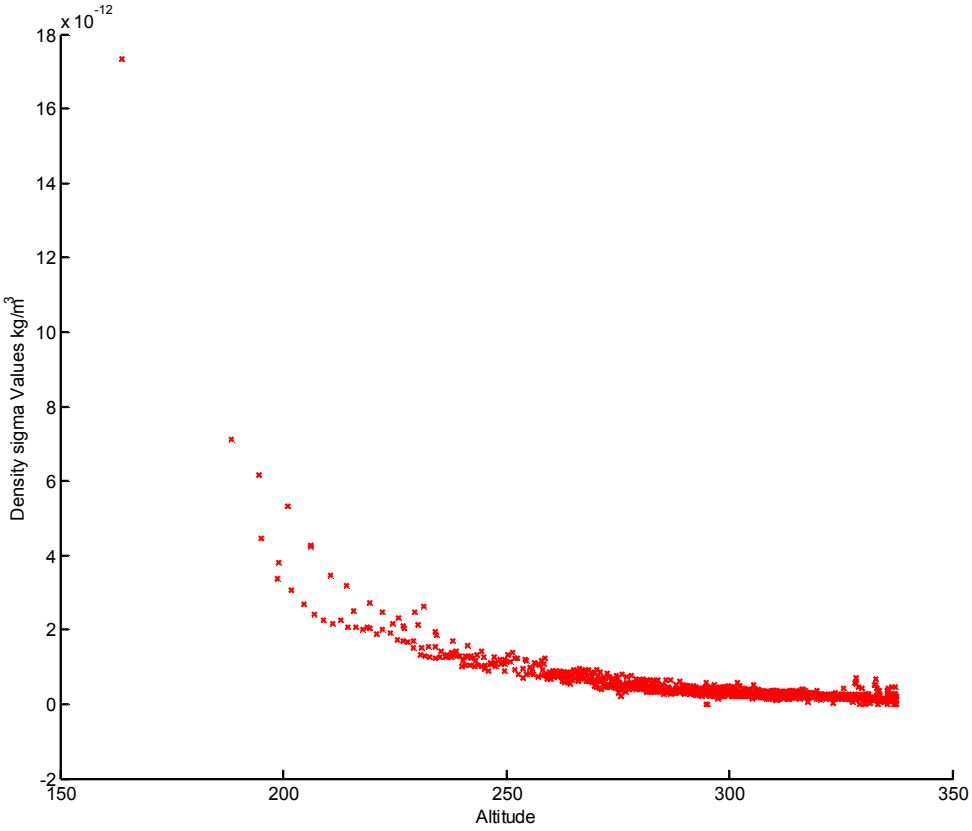

Figure 3.18: Density Uncertainty Dependence on Altitude

In Figure 3.18 density uncertainty is examined for all of the ANDE satellites during the course of their lifespan, and as their orbits decayed. As the orbits decay, density uncertainty increases while actual density values also increase. In future graphs, uncertainty as a percentage of the derived values for density is also examined to reduce bias that may be caused due to altitude.

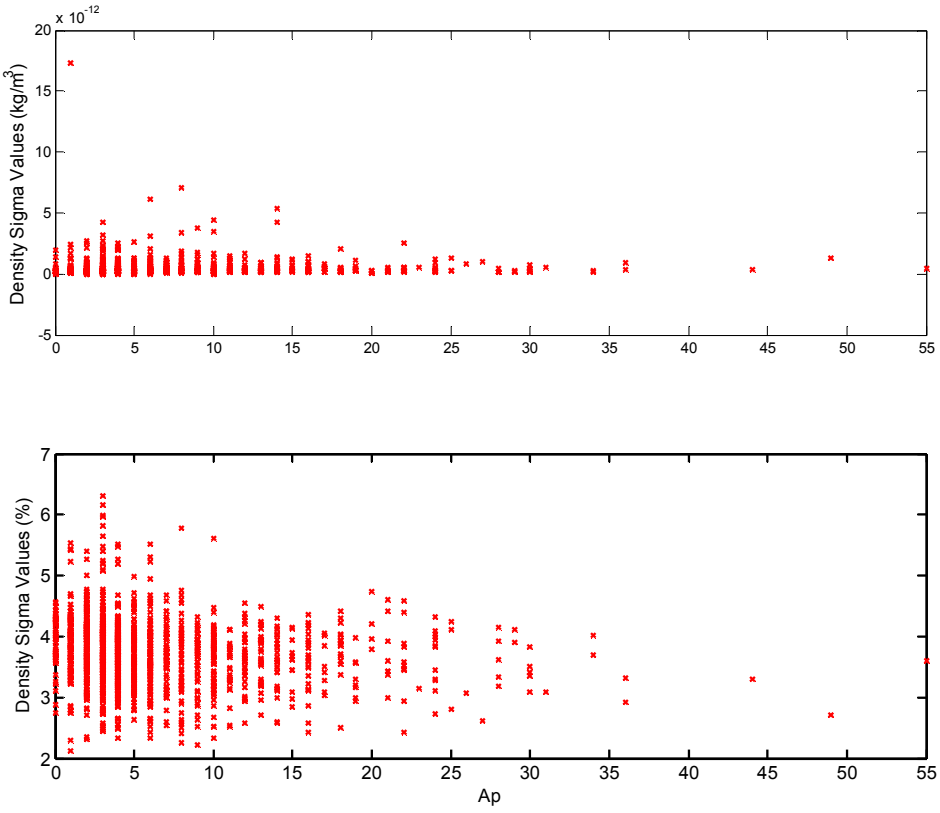

Figure 3.19: Density Uncertainty Dependence on Geomagnetic Activity

In Figure 3.19, density uncertainty has no clear trends due to geomagnetic activity, with most of the uncertainties being around 4%. There is a wider spread at low A_p values, but this is likely due to a larger data set for that level of geomagnetic activity.

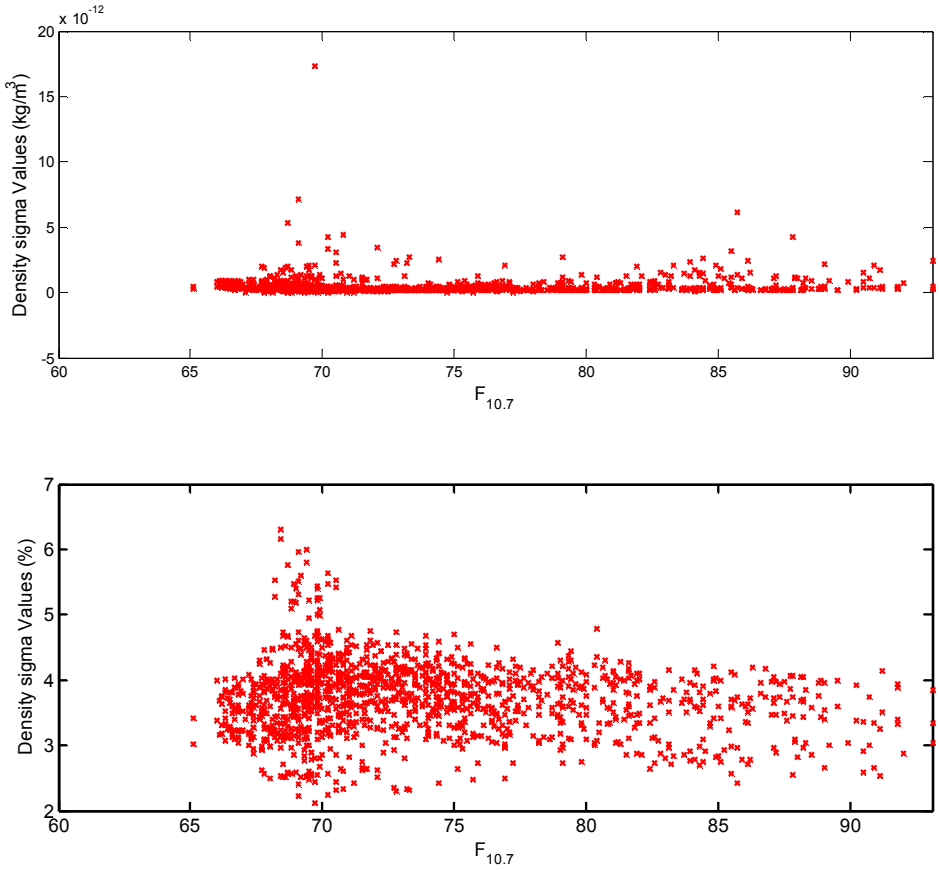

Figure 3.20: Density Uncertainty Dependence on Solar Activity

In Figure 3.20 density uncertainty does appear to have a slight dependence on solar activity. Density uncertainty appears to increase to a maximum around a value of 68 or 69 for solar flux, and then appears to taper off.

3.5 Preliminary SPINSAT Results

SPINSAT was launched in September 2014 to the International Space Station, and was deployed on November 28, 2014; data is now available for SPINSAT in the same forms as it was for the rest of the ANDE satellites, from December 2014 onward. What follows is a sample of density corrections obtained so far from SPINSAT.

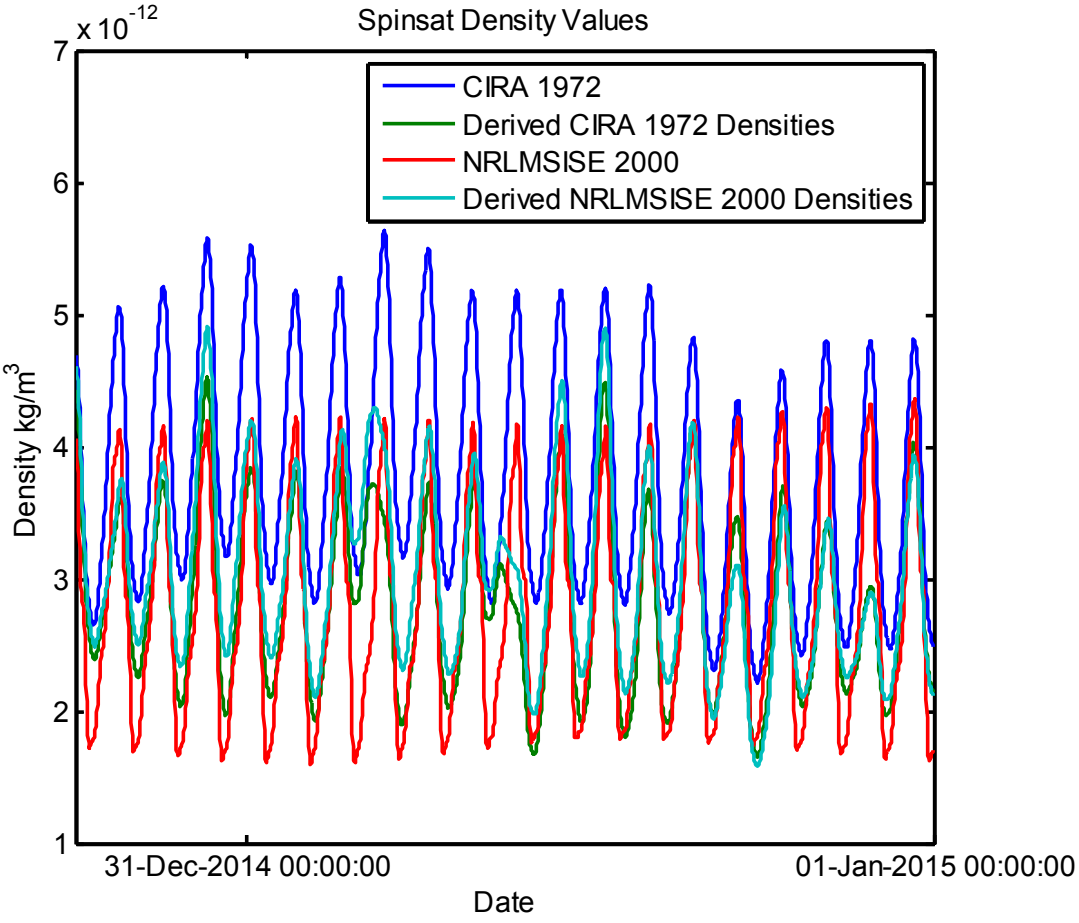

Figure 3.21: SPINSAT Model and Derived Densities for December 31, 2014

In Figure 3.21, the regular sine wave pattern for atmospheric density values perceived by the satellite is seen in both the atmospheric model predicted densities, as well as the derived densities utilizing orbit data to make corrections to the models. There does appear to be an anomaly near the middle of the arc which may be due to usage of SPINSAT's maneuvering thruster. December 31 was chosen as it was further into the satellite lifespan, and hence, the satellite would hopefully be more stable in its orbit at this point.

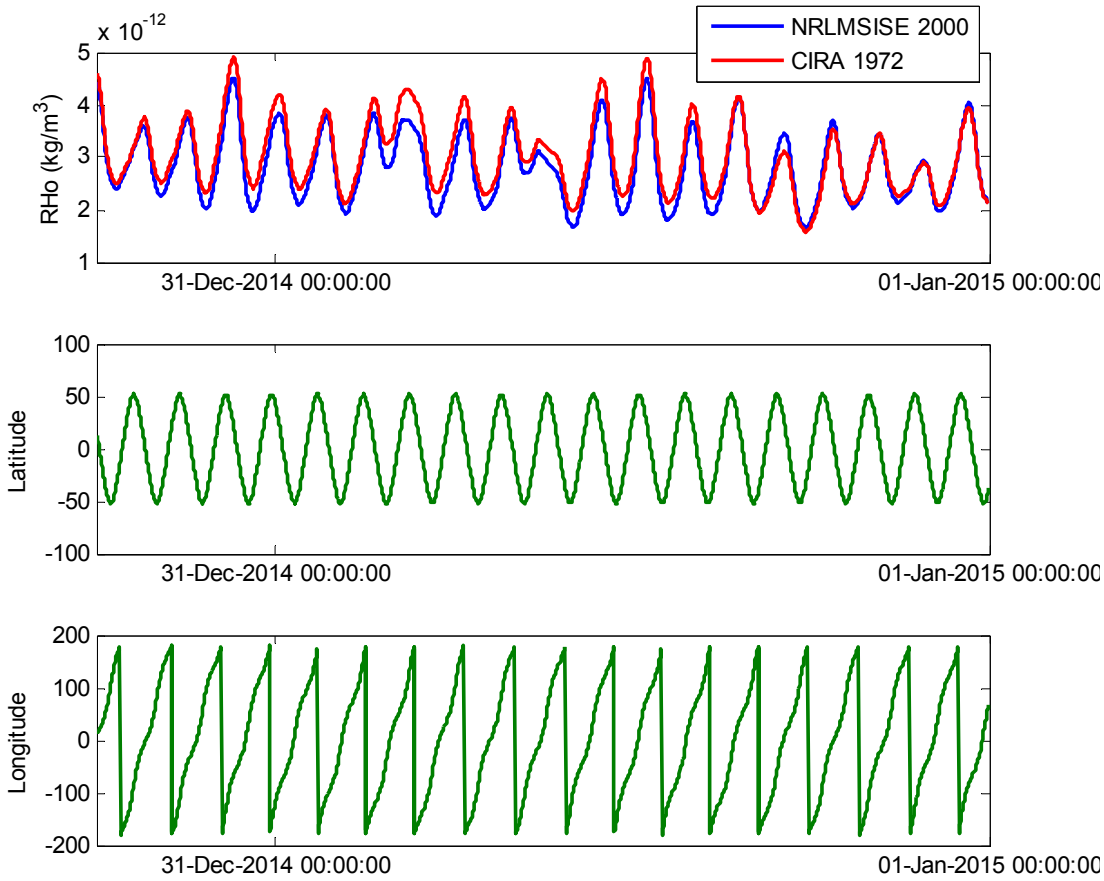

Figure 3.22: Derived SPINSAT Atmospheric Densities, and Corresponding Geographic Locations for December 31, 2014

Figure 3.22 shows identical derived densities to those appearing in Figure 3.21, with the corresponding geographic location of SPINSAT at the time. During the density anomaly observed on December 31, 2014, SPINSAT appears to have been above North America at the time, giving credence to the hypothesis that the anomaly may have been due to a maneuver. Over the lifespan of SPINSAT, additional corrections to atmospheric density may be determined, as well as, possibly identifying maneuvers occurring during flight through anomaly detection.

4 Conclusions and Future Work

This work established the validity of using SLR data sets to estimate atmospheric densities by comparing results for the ANDE Castor satellite to results for the CHAMP and GRACE satellites for the same time periods. The density correction factors and standard deviations comparing the baseline model densities to the derived atmospheric densities are also examined for the ANDE Castor satellite. For the entire family of ANDE satellites, the uncertainty in atmospheric density is established for each arc. The uncertainties are significantly higher at the beginning of the arc for each of the satellites, and the uncertainties also increase as the satellites drop in altitude. Density values for the SPINSAT satellite are also estimated.

To continue this work, SPINSAT should be examined during its operational lifespan, given its similarity in form and function to the ANDE satellites, as well as its operational lifetime occurring during higher levels of solar and geomagnetic activity than were observed during the ANDE missions' lives. In the future, an excellent goal would be to procure NRL ephemeris and density data for the ANDE satellites, and use it for comparison purposes against data generated using SLR measurements.

Extended satellite life-spans of the GRACE satellites mean that there is additional data to be analyzed, that has not previously been covered. POE data are also available for the TerraSAR-X satellite, which can provide another source of highly accurate data with which to formulate corrections to existing atmospheric density models. In addition to these sources of highly precise data, there is also precise data available from the Jet Propulsion Laboratory (JPL), for CHAMP, GRACE, TerraSAR-X, and many other satellites.

Given that SPINSAT is a test bed for a form of propulsion, examination of derived density values may result in anomalies in the estimated densities. These values will likely have little use in formulating corrections to existing atmospheric models, but may prove useful in the identification of maneuvers by other satellites.

Upon incorporation of the aforementioned satellites, other satellites may be incorporated as needed or available in this research. The final goal to assimilate these corrected density values into existing general circulation models, such as the Global Ionosphere/Thermosphere Model (GITM), and the Thermosphere-Ionosphere-Electrodynamics General Circulation Model (TIE-GCM). With the assimilation of the density values, the effects of their inclusion in global models may be observed.

REFERENCES

[1] D. A. Vallado, *Fundamentals of Astrodynamics and Applications*, Microcosm Press, El Segundo, CA, 3rd Edition, 2007, Chap. 8, App. B.

[2] B. Bowman, F. A. Marcos, and M. J. Kendra, "A Method for Computing Accurate Atmospheric Density Values from Satellite Drag Data," *Advances in the Astronautical Sciences*, Vol. 119, AAS 04-173, Univelt, 2004, pp. 1117-1134.

[3] L. G. Jacchia, *Revised Static Models for the Thermosphere and Exosphere with Empirical Temperature Profiles*, SAO Special Report No. 332, Smithsonian Institution Astrophysical Observatory, Cambridge, MA, 1971.

[4] C. E. Roberts, Jr., "An Analytic Model for Upper Atmosphere Densities Based upon Jacchia's 1970 Models," *Celestial Mechanics*, Vol. 4, Issue 3-4, December 1971, pp. 368-377.

[5] COSPAR Working Group IV, *COSPAR International Reference Atmosphere*, Akademie-Verlag, Berlin, 1972.

[6] A. E. Hedin, "Extension of the MSIS Thermosphere Model into the Middle and Lower Atmosphere," *Journal of Geophysical Research*, Vol. 96, 1991, pp. 1159-1172.

[7] J.M. Picone, A. E. Hedin, D. P. Drob, "NRLMSISE-00 Empirical Model of the Atmosphere: Statistical Comparisons and Scientific Issues," *Journal of Geophysical Research*, Vol. 107, No. A12, 2002.

[8] B. R. Bowman, W. K. Tobiska, F. A. Marcos, C. Y. Huang, C. S. Lin, W. J. Burke, "A New Empirical Thermospheric Density Model JB2008 Using New Solar and Geomagnetic Indices," AIAA 2008-6438, AIAA/AAS Astrodynamics Specialist Conference, Honolulu, HI, August 2008.

[9] National Geophysical Data Center, *Solar Indices Bulletin*, Boulder, CO: National Geophysical Data Center, http://www.ngdc.noaa.gov/ and ftp://ftp.ngdc.noaa.gov/STP/SOLAR_DATA/SOLAR_RADIO/FLUX.

[10] National Geophysical Data Center, *Solar Indices Bulletin*, Boulder, CO: National Geophysical Data Center, http://www.ngdc.noaa.gov/ and ftp://ftp.ngdc.noaa.gov/STP/GEOMAGNETIC_DATA/INDICES/KP_AP/.

[11] M. F. Storz, B. R. Bowman, Major J. I. Branson, S. J. Casali, and W. K. Tobiska, "High Accuracy Satellite Drag Model (HASDM)," *Advances in Space Research*, Vol. 36, Issue 12, 2005, pp. 2497-2505.

[12] B. Bowman, "The Semiannual Thermospheric Density Variation from 1970 to 2002 Between 200-1100 km," *Advances in the Astronautical Sciences*, Vol. 119, AAS 04-174, Univelt, 2004, pp. 1135-1154.

[13] P. J. Cefola, R. J. Proulx, A. I. Nazarenko, and V. S. Yurasov, "Atmospheric Density Correction Using Two Line Element Sets as the Observation Data," *Advances in the Astronautical Sciences*, Vol. 116, AAS 03-626, Univelt, 2003, pp. 1953-1978.

[14] V. S. Yurasov, A. I. Nazarenko, P. J. Cefola, and K. T. Alfriend, "Results and Issues of Atmospheric Density Correction," *Journal of the Astronautical Sciences*, Vol. 52, No. 3, July-September 2004, pp. 281-300

[15] V. S. Yurasov, A. I. Nazarenko, K. T. Alfriend, and P. J. Cefola, "Reentry Time Prediction Using Atmospheric Density Corrections," *Journal of Guidance, Control, and Dynamics*, Vol. 31, No. 2, March-April 2008, pp. 282-289.

[16] M. P. Wilkins, C. A. Sabol, P. J. Cefola, and K. T. Alfriend, "Practical Challenges in Implementing Atmospheric Density Corrections to the NRLMSISE-00 Model," *Advances in the Astronautical Sciences*, Vol. 124, AAS 06-170, Univelt 2006, pp. 1113-1130.

[17] M. P. Wilkins, C. A. Sabol, P. J. Cefola, and K. T. Alfriend, "Improving Dynamic Calibration of the Atmosphere," *Advances in the Astronautical Sciences*, Vol. 127, AAS 07-185, Univelt, 2007, pp. 1257-1272.

[18] M. P. Wilkins, C. A. Sabol, P. J. Cefola, and K. T. Alfriend, "Validation and Application of Corrections to the NRLMSISE-00 Atmospheric Density Model," *Advances in the Astronautical Sciences*, Vol. 127, AAS 07-189, Univelt, 2007, pp. 1285-1304.

[19] S. R. Mance, C. A. McLaughlin, F. G. Lemoine, D. D. Rowlands, and P. J. Cefola, "GEOSAT Follow-On Precision Orbit Improvement Through Drag Model Update," *Advances in the Astronautical Sciences,* Vol. 134, AAS 09-105, Univelt, 2009, pp. 43-62.

[20] E. Doornbos, H. Klinkrad, and P. Visser, "Use of Two-Line Element Data for Thermosphere Neutral Density Model Calibration," *Advances in Space Research*, Vol. 41, 2008, pp. 1115-1122.

[21] R. Konig and K. H. Neumayer, "Thermospheric Events in CHAMP Precise Orbit Determination," *First CHAMP Mission Results for Gravity, Magnetic and Atmospheric Studies*, eds. C. Reigber, H. Luhr, P. Schwintzer, Springer, Berlin, 2003, pp. 112-119.

[22] S. Bruinsma and R. Biancale, "Total Density Retrieval with STAR," *First CHAMP Mission Results for Gravity, Magnetic and Atmospheric Studies*, eds. C. Reigber, H. Luhr, P. Schwintzer, Springer, Berlin, 2003, pp. 192-199.

[23] S. Bruinsma and R. Biancale, "Total Densities Derived from Accelerometer Data," *Journal of Spacecraft and Rockets*, Vol. 40, No. 2, March-April 2003, pp. 230-236.

[24] S. Bruinsma, S. D. Tamagnan and R. Biancale, "Atmospheric Densities Derived from CHAMP/STAR Accelerometer Observations," *Planetary and Space Science*, Vol. 52, 2004, pp. 297-312.

[25] E. K. Sutton, R. S. Nerem, and J. M. Forbes, "Global Thermospheric Neutral Density and Wind Response to the Severe 2003 Geomagnetic Storms from CHAMP Accelerometer Data," *Journal of Geophysical Research*, Vol. 110, 2005.

[26] J. M. Forbes, G. Lu, S. Bruinsma, S. Nerem, and X. Zhang, "Thermospheric Density Variations Due to the 15-24 April 2002 Solar Events from CHAMP/STAR Accelerometer Measurements," *Journal of Geophysical Research*, Vol. 110, 2005, pp. 1-9.

[27] E. K. Sutton, J. M. Forbes, R. S. Nerem, and T. N. Woods, "Neutral Density Response to the Solar Flares of October and November, 2003," *Geophysical Research Letters*, Vol. 33, 2006.

[28] S. Bruinsma, J. M. Forbes, R. S. Nerem, and X. Zhang, "Thermospheric Density Response to the 20-21 November 2003 Solar and Geomagnetic Storm from CHAMP and GRACE Accelerometer Data," *Journal of Geophysical Research*, Vol. 111, No. AO6303, 2006, pp. 1-14.

[29] S. L. Bruinsma and J. M. Forbes, "Storm-Time Equatorial Density Enhancements Observed by CHAMP and GRACE," *Journal of Spacecraft and Rockets*, Vol. 44, No. 6, 2007, pp. 1154-1159.

[30] E. K. Sutton, R. S. Nerem, and J. M. Forbes, "Density and Winds in the Thermosphere Deduced from Accelerometer Data," *Journal of Spacecraft and Rockets*, Vol. 44, No. 6, 2007, pp. 1210-1219.

[31] B. D. Tapley, J. C. Ries, S. Bettadpur, and M. Cheng, "Neutral Density Measurements for the Gravity Recovery and Climate Experiment Accelerometers," *Journal of Spacecraft and Rockets*, Vol. 44, No. 6, 2007, pp. 1220-1225.

[32] S. L. Bruinsma and J. M. Forbes, "Medium- to Large-Scale Density Variability as Observed by CHAMP," *Space Weather*, Vol. 6, S08002, doi:10.1029/2008SW000411, 2008.

[33] Y. L. Zhou, S. Y. Ma, H. Lühr, C. Xiong, and C. Reigber, "An Empirical Relation to Correct Storm-Time Thermospheric Mass Density Modeled by NRLMSISE-00 with CHAMP Satellite Air Drag Data," *Advances in Space Research*, Vol. 43, 2009, pp. 819-828.

[34] Zhang, J. T., J. M. Forbes, C. H. Zhang, E. Doornbos, and S. L. Bruinsma (2014), Lunar tide contribution to thermosphere weather, *Space Weather*, *12*, 538–551, doi:10.1002/2014SW001079.

[35] Häusler, K., M. E. Hagan, A. J. G. Baumgaertner, A. Maute, G. Lu, E. Doornbos, S. Bruinsma, J. M. Forbes, and F. Gasperini (2014), Improved short-term variability in the thermosphere-ionospheremesosphere-electrodynamics general circulation model, *J. Geophys. Res. Space Physics*, *119*, 6623–6630, doi:10.1002/2014JA020006.

[36] E. Doornbos, H. Klinkrad, and P. Visser, "Atmospheric Density Calibration Using Satellite Drag Observations," *Advances in Space Research*, Vol. 36, 2005, pp. 515-521.

[37] J. van den Ijssel, P. Visser, and R. Haagmans, "Determination of Non-Conservative Accelerations from Orbit Analysis," *Earth Observation with CHAMP Results from Three Years in Orbit*, eds. C. Reigber, H. Luhr, P. Schwintzer, J. Wickert, Springer, Berlin, 2005, pp. 95-100.

[38] J. van den IJssel and P. Visser, "Determination of Non-Gravitational Accelerations from GPS Satellite-to-Satellite Tracking of CHAMP," *Advances in Space Research*, Vol. 36, 2005, pp. 418-423.

[39] J. van den IJssel and P. Visser, "Performance of GPS-Based Accelerometry: CHAMP and GRACE," *Advances in Space Research*, Vol. 39, 2007, pp. 1597-1603.

[40] O. Montenbruck, T. van Helleputte, R. Kroes, and E. Gill, "Reduced Dynamic Orbit Determination Using GPS Code and Carrier Measurements," *Aerospace Science and Technology*, Vol. 9, 2005, pp. 261-271.

[41] P. Willis, F. Deleflie, F. Barlier, Y. E. Bar-Sever, and L. J. Romans, "Effects of Thermosphere Total Density Perturbations on LEO Orbits During Severe Geomagnetic Conditions (Oct-Nov 2003) Using DORIS and SLR Data," *Advances in Space Research*, Vol. 36, 2005, pp. 522-533.

[42] C. A. McLaughlin and B. S. Bieber, "Neutral Density Determined from CHAMP Precision Orbits," *Advances in the Astronautical Sciences*, Vol. 129, AAS 07-260, Univelt, 2008, pp. 167-186.

[43] C. A. McLaughlin, A. Hiatt, and B. S. Bieber, "Comparison of Total Density Derived from CHAMP Precision Orbits and CHAMP Accelerometer," *Advances in the Astronautical Sciences*, Vol. 130, AAS 08-177, Univelt, 2008, pp. 1193-1206.

[44] C. A. McLaughlin, A. Hiatt, T. Lechtenberg, "Calibrating Precision Orbit Derived Total Density," AIAA 2008-6951, *2008 AIAA/AAS Astrodynamics Specialist Conference and Exhibit*, Honolulu, HI, August 2008.

[45] Hiatt A., "Deriving Atmospheric Density Estimates Using Satellite Precision Orbit Ephemerides," M. S. Thesis, Department of Aerospace Engineering, University of Kansas, 2009.

[46] Lechtenberg T., "Derivation and Observability of Upper Atmospheric Density Variations Utilizing Precision Orbit Ephemerides," M. S. Thesis, Department of Aerospace Engineering, University of Kansas, 2010.

[47] McLaughlin, C. A., T. F. Lechtenberg, S. R. Mance, T. Locke, and P. M. Mehta, "Fitted Drag Coefficients as a Source of Density Information," *Space Flight Mechanics 2011*, Vol. 140 of *Advances in the Astronautical Sciences*, AAS 11-174, pp. 1057-1074, 2011.

[48] McLaughlin, C. A., S. Mance, and T. Lechtenberg, "Drag Coefficient Estimation in Orbit Determination," *Journal of the Astronautical Sciences*, Vol. 58, No. 3, Part 2, 2011, pp. 513-530.

[49] Fattig, E., McLaughlin, C. A., and T. Lechtenberg, "Comparison of Density Estimation for CHAMP and GRACE Satellites," *AIAA/AAS Astrodynamics Specialist Conference*, Toronto, ON, AIAA 2010-7976, 2-5 August 2010.

[50] McLaughlin, C. A., T. Lechtenberg, and E. Fattig, "Estimating Density Using Precision Satellite Orbits from Multiple Satellites," *Kyle T. Alfriend Astrodynamics Symposium*, Vol. 139 of *Advances in the Astronautical Sciences,* 2010, AAS 10-307, pp. 87-102.

[51] McLaughlin, C. A., A. Hiatt, and T. Lechtenberg, "Precision Orbit Derived Total Density," *Journal of Spacecraft and Rockets*, Vol. 48, No. 1, January-February, 2011, pp. 166-174.

[52] McLaughlin, C. A., T. Lechtenberg, E. Fattig, D. Mysore Krishna, "Estimating Density Using Precision Satellite Orbits from Multiple Satellites," *Journal of the Astronautical Sciences*, Vol. 59, No. 1-2, 2012, pp. 85-101.

[53] Mysore Krishna, D., "Improving and Expanding Orbit Derived Atmospheric Densities," M. S. Thesis, Department of Aerospace Engineering, University of Kansas, 2012.

[54] McLaughlin, C. A., A. Hiatt, D. Mysore Krishna, T. Lechtenberg, E. Fattig, and P. M. Mehta, "Precision Orbit Derived Atmospheric Density: Development and Performance," *Advanced Maui Optical and Space Surveillance Technologies Conference*, Maui, HI, September 12-14, 2012.

[55] Lechtenberg, T. F., C. A. McLaughlin, T. Locke, and D. Mysore Krishna, "Thermospheric Density Variations: Observability using Precision Satellite Orbits and Effects on Orbit Propagation," *Space Weather*, Vol. 11, pp. 34-45, doi:10.1029/2012SW000848.

[56] B. D. Tapley, B. E. Schutz, and G. H. Born, *Statistical Orbit Determination*, Elsevier Academic Press, Amsterdam, 2004.

[57] J. R. Wright, "Real-Time Estimation of Local Atmospheric Density," *Advances in the Astronautical Sciences*, Vol. 114, AAS 03-164, Univelt, 2003, pp. 927-950.

[58] J. R. Wright and J. Woodburn, "Simultaneous Real-Time Estimation of Atmospheric Density and Ballistic Coefficient," *Advances in the Astronautical Sciences*, Vol. 119, AAS 04-175, Univelt, 2004, pp. 1155-1184.

[59] C. A. McLaughlin, A. Hiatt, E. Fattig, and T. Lechtenberg, "Ballistic Coefficient and Density Estimation," *Astrodynamics 2009*, Vol. 135 of *Advances in the Astronautical Sciences*, 2009, AAS 09-439, pp. 2269-2285.

[60] P. M. Mehta, C. A. McLaughlin, E. K. Sutton, "Drag coefficient modeling for grace using Direct Simulation Monte Carlo," *Advances in Space Research*, Vol. 52, Pages 2035-2051, http://dx.doi.org/10.1016/j.asr.2013.08.033.

[61] Earth Observation Portal, "CHAMP," Last Accessed: July 1, 2014. URL: https://directory.eoportal.org/web/eoportal/satellite-missions/c-missions/champ

[62] Airbus Defence & Space, "Champ," Last Accessed: July 8, 2014. URL: http://www.space-airbusds.com/en/programme/champ-cta.html.

[63] GRACE: Gravity Recovery and Climate Experiment: Center for Space Research, "GRACE Orbital Configuration," August 2, 2007, Last Accessed: April 14, 2010, http://www.csr.utexas.edu/grace/operations/configuration.html.

[64] Earth Observation Portal, "ANDE," Last Accessed: July 8, 2014. URL: https://directory.eoportal.org/web/eoportal/satellite-missions/a/ande.

[65] L. Thomas, "ANDE Concept," 16th International Workshop on Laser Ranging, Poznan Poland, October 2008. URL: http://cddis.gsfc.nasa.gov/lw16/docs/presentations/ops_14_Thomas.pdf

[66] "ANDE Mission Page," *ILRS*, http://ilrs.gsfc.nasa.gov/missions/satellite_missions/past_missions/anda_general.html, Last Accessed: 1/31/14.

[67] Andrew C. Nicholas, Ted Fine, Mark A. Davis, Robert Kessel, "Atmospheric Neutral Density Experiment (ANDE-2) Flight Hardware Details," May 26, 2009, URL: http://ilrs.gsfc.nasa.gov/docs/andehw.pdf.

[68] Nicholas, A. C., J.M. Picone, J. Emmert, J. DeYoung, L. Healy, L. Wasiczko, M. Davis and C. Cox, Preliminary Results from the Atmospheric Neutral Density Experiment Risk Reduction Mission. In *Proc. of the AAS/AIAA Astrodynamics Specialist Conference,* AAS 07-265.

[69] Nicholas, Andrew, Ted Finne, Ivan Galysh, Anthony Mai, Jim Yen, Wayne Sawka, Jeff Ransdell, Shae Williams, "SpinSat Mission Overview," Proceedings of the 27th AIAA/USU Conference, Small Satellite Constellations, Logan, Utah, USA, Aug. 10-15, 2013, paper: SSC13-I-3, URL:http://digitalcommons.usu.edu/cgi/viewcontent.cgi?article=2911&context=smallsat

[70] B. R. Bowman, F. A. Marcos, K. Moe, M. M. Moe, "Determination of Drag Coefficient Values for CHAMP and GRACE Satellites Using Orbit Drag Analysis," *Advances in the Astronautical Sciences*, Vol. 129, AAS 07-259, Univelt, 2008, pp. 147-166.

[71] Andrew Walker, Piyush Mehta, and Josef Koller. "Drag Coefficient Model Using the Cercignani–Lampis–Lord Gas–Surface Interaction Model", Journal of Spacecraft and Rockets, Vol. 51, No. 5 (2014), pp. 1544-1563. doi: 10.2514/1.A32677.

[72] R. Konig, S. Zhu, C. Reigber, K. H. Neumayer, H. Meixner, R. Galas, G. Baustert, "CHAMP Rapid Orbit Determination for GPS Atmospheric Limb Sounding," *Advances in Space Research*, Vol. 30, No. 2, 2002, pp. 289-293.

[73] G. Michalak, G. Baustert, R. Konig, C. Reigber, "CHAMP Rapid Science Orbit Determination: Status and Future Prospects," *First CHAMP Mission Results for*

Gravity, Magnetic and Atmospheric Studies, eds. C. Reigber, H. Luhr, P. Schwintzer, Springer, Berlin, 2003, pp. 98-103.

[74] R. Konig, G. Michalak, K. H. Neumayer, S. Y. Zhu, H. Meixner, C. Reigber, "Recent Developments in CHAMP Orbit Determination at GFZ," *Earth Observation with CHAMP Results from Three Years in Orbit*, eds. C. Reigber, H. Luhr, P. Schwintzer, J. Wickert, Springer, Berlin, 2005, pp. 65-70.

[75] R. Konig, G. Michalak, K. H. Neumayer, S. Zhu, "Remarks on CHAMP Orbit Products," *Observation of the Earth System from Space*, eds. J. Flury, R. Rummel, C. Reigber, M. Rothacher, G. Boedecker, U. Schreiber, Springer, Berlin, 2006, pp. 17-26.

[76] O. Montenbruck and E. Gill, *Satellite Orbits: Models, Methods, and Applications*, Springer-Verlag, Berlin, 2001.

[77] J. R. Wright, "Optimal Orbit Determination," *Advances in the Astronautical Sciences*, Vol. 112, AAS 02-192, Univelt, 2002, pp. 1123-1134, http://www.agi.com/downloads/support/productSupport/literature/pdfs/whitePapers/optimal_od.pdf.

[78] Analytical Graphics, Inc., "Orbit Determination Tool Kit Help," *Orbit Determination Tool Kit*, Version 5.1.4.

[79] B. R. Bowman, F. A. Marcos, K. Moe, M. M. Moe, "Determination of Drag Coefficient Values for CHAMP and GRACE Satellites Using Orbit Drag Analysis," *Advances in the Astronautical Sciences*, Vol. 129, AAS 07-259, Univelt, 2008, pp. 147-166.